Abnormal brain state distribution and network connectivity in a SYNGAP1 rat model

OXFORD UNIVERSITY PRESS | Brain Communications

Abnormal brain state distribution and network connectivity in a SYNGAP1 rat model

Journal:	*Brain Communications*
Manuscript ID	BRAINCOM-2022-043.R2
Manuscript Type:	Original Article
Date Submitted by the Author:	09-Jul-2022
Complete List of Authors:	Buller-Peralta, Ingrid; The University of Edinburgh Centre for Discovery Brain Sciences, Simons Initiative for the Developing Brain, Patrick Wild Centre Maicas-Royo, Jorge; The University of Edinburgh Centre for Discovery Brain Sciences, Simons Initiative for the Developing Brain, Patrick Wild Centre Lu, Zhuoen; The University of Edinburgh, School of Engineering, Institute for Digital Communications, EH93JL Till, Sally; The University of Edinburgh Centre for Discovery Brain Sciences, Simons Initiative for the Developing Brain, Patrick Wild Centre Wood, Emma; The University of Edinburgh Centre for Discovery Brain Sciences, Simons Initiative for the Developing Brain, Patrick Wild Centre Kind, Peter; The University of Edinburgh Centre for Discovery Brain Sciences, Simons Initiative for the Developing Brain, Patrick Wild Centre escudero, javier; The University of Edinburgh, School of Engineering, Institute for Digital Communications, EH93JL Gonzalez-Sulser, Alfredo; The University of Edinburgh Centre for Discovery Brain Sciences, Simons Initiative for the Developing Brain, Patrick Wild Centre
Keywords:	Syngap1, EEG, Connectivity, Epileptic Encephalopathy, Sleep

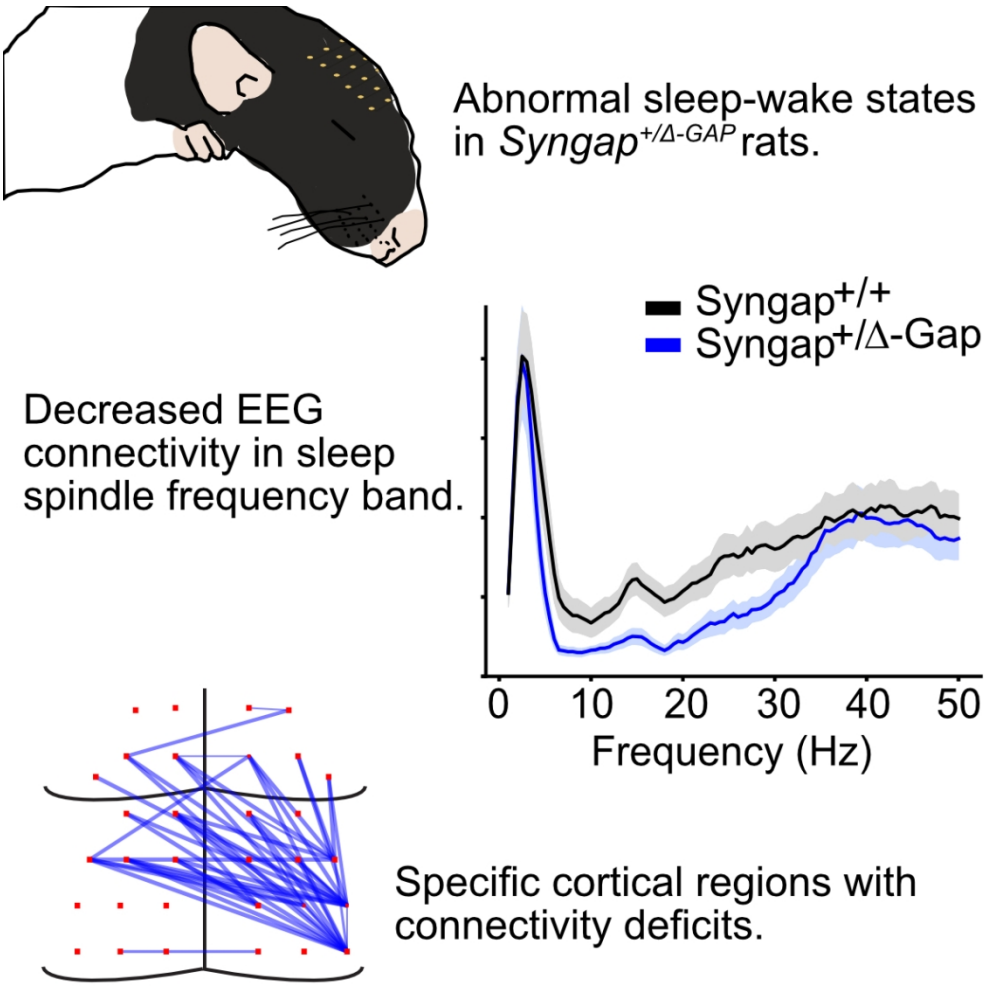

Graphica Abstract: Buller-Peralta et al., found sleep and connectivity deficits in a rat model of SYNGAP1 haploinsufficiency from multi-channel EEG recordings. Mutants displayed altered brain state distributions and decreased connectivity between short distance electrodes during NREM. Mutants had decreased high connectivity instances during sleep spindles, which was specific to certain cortical electrodes.

Abbreviated Summary

Buller-Peralta et al., found sleep and connectivity deficits in a rat model of *SYNGAP1* haploinsufficiency from multi-channel EEG recordings. Mutants displayed altered brain state distributions and decreased connectivity between short distance electrodes during NREM. Mutants had decreased high connectivity instances during sleep spindles, which was specific to certain cortical electrodes.

Abnormal brain state distribution and network connectivity in a *SYNGAP1* rat model

Ingrid Buller-Peralta*[1], Jorge Maicas-Royo*[1], Zhuoen Lu*[2], Sally M. Till[1], Emma R. Wood[1], Peter C. Kind[1], Javier Escudero[2], Alfredo Gonzalez-Sulser[1]

Affiliations: [1]Simons Initiative for the Developing Brain, Patrick Wild Centre, Centre for Discovery Brain Sciences, University of Edinburgh, Edinburgh, United Kingdom EH8 9XD; [2]School of Engineering, Institute for Digital Communications, University of Edinburgh, Edinburgh, United Kingdom EH9 3JL.

* = Equal contribution.

Corresponding author:

Alfredo Gonzalez-Sulser
Simons Initiative for the Developing Brain Fellow
University of Edinburgh
Centre for Discovery Brain Sciences
1 George Square
Edinburgh, EH89JZ
United Kingdom
Tel: +44-1316511903
Email: agonzal2@ed.ac.uk

Short Title: Altered sleep and EEG coherence in *SYNGAP1* rats

Abstract

Mutations in the *SYNGAP1* gene are one of the common predictors of neurodevelopmental disorders, commonly resulting in individuals developing autism, intellectual disability, epilepsy, and sleep deficits. EEG recordings in neurodevelopmental disorders show potential to identify clinically translatable biomarkers to both diagnose and track the progress of novel therapeutic strategies, as well as providing insight into underlying pathological mechanisms. In a rat model of *SYNGAP1* haploinsufficiency in which the exons encoding the calcium/lipid binding and GTPase activating protein domains have been deleted (*Syngap*$^{+/\Delta\text{-}GAP}$) we analysed the duration and occurrence of wake, non rapid eye movement and rapid eye movement brain states during 6 hour multi-electrode EEG recordings. We find that although *Syngap*$^{+/\Delta\text{-}GAP}$ animals spend an equivalent percent time in wake and sleep states, they have an abnormal brain state distribution as the number of wake and non rapid eye movement bouts are reduced and there is an increase in the average duration of both wake and non rapid eye movement epochs. We perform connectivity analysis by calculating the average imaginary coherence between electrode pairs at varying distance thresholds during these states. In group averages from pairs of electrodes at short distances from each other, a clear reduction in connectivity during non rapid eye movement is present between 11.5 Hz and 29.5 Hz, a frequency range that overlaps with sleep spindles, oscillatory phenomena thought to be important for normal brain function and memory consolidation. Sleep abnormalities were mostly uncorrelated to the electrophysiological correlate of absence seizures, spike and wave discharges, as was the imaginary coherence deficit. Sleep spindles occurrence, amplitude, power and spread across multiple electrodes were not reduced in *Syngap*$^{+/\Delta\text{-}GAP}$ rats, with only a small decrease in duration detected. Nonetheless, by analysing the dynamic imaginary coherence during sleep spindles, we found a reduction in high connectivity instances between short-distance electrode pairs. Finally comparing the dynamic imaginary coherence during sleep spindles between individual electrode pairs, we identified a group of channels over the right somatosensory, association and visual cortices that have a significant reduction in connectivity during sleep spindles in mutant animals. This matched significant reduction in connectivity during spindles when averaged regional comparisons were made. These data suggest that *Syngap*$^{+/\Delta\text{-}GAP}$ rats

have altered brain state dynamics and EEG connectivity, which may have clinical relevance for *SYNGAP1* haploinsufficiency in humans.

Keywords: SYNGAP1, EEG, connectivity, Epileptic Encephalopathy, Sleep.

Abbreviations: C2, GAP, ID, NDD, NREM, REM, and SWD.

Introduction

Neurodevelopmental disorders (NDDs) encompass multiple disease phenotypes that are linked to a highly heterogenous genetic architecture[1]. Mutations in the *SYNGAP1* gene account for as many as 1% of NDD cases, with patients often presenting with intellectual disability (ID) and autism spectrum disorder[2–6]. Most patients with *SYNGAP1* pathogenic variants display some form of epilepsy with a high prevalence of absence seizures and a behavioural developmental delay occurring upon seizure onset. Therefore, *SYNGAP1* haploinsufficiency is often classed as an epileptic encephalopathy[3,7,8]. Additionally, sleep impairments have been reported by parents [3] and have been documented in the clinical setting in a high proportion of cases[8,9].

Characterization of novel biomarkers of NDDs may allow for early diagnosis and rapid therapeutic intervention, enabling quantitative monitoring of treatment efficacy, which is likely critical for the success of future clinical trials[10]. EEG recordings are a potentially reliable method of identifying biomarkers as they provide a fast and direct measure of overall brain activity[11]. However, given the heterogeneity of aetiologies, phenotypes and disease trajectories of NDDs, biomarkers specific for particular genetic disorders such as *SYNGAP1* are imperative to differentiate between NDD types and identify likely disease outcomes[12].

The rare incidence of NDD patients with specific mutations makes performing large-cohort EEG studies to identify biomarkers difficult. *SYNGAP1* haploinsufficiency cases are thought to occur in only 6.1 per 100,000 people[13]. Identifying clinically relevant biomarkers in genetically modified rodent models of NDDs is a plausible alternative strategy. Furthermore, these biomarkers may then converge and be applicable to other NDD types.

SYNGAP1 encodes a Ras-GTPase-activating protein, which is mainly expressed in the synapses of excitatory neurons[14,15]. It is a key regulator of the postsynaptic density and in synaptic development and plasticity[16]. We recently reported on a novel rat model of *SYNGAP1* haploinsufficiency in which the calcium/lipid binding (C2) and GTPase activating (GAP) domains, areas thought to be critical for the normal function of SYNGAP, have been deleted[17]. Animals heterozygous for the C2/GAP domain deletion (*Syngap*$^{+/\Delta\text{-}GAP}$) displayed reduced exploration and fear extinction, altered social behaviour and spontaneous absence seizures. SYNGAP plays a critical role in synaptic transmission and organisation, therefore we hypothesize that *Syngap*$^{+/\Delta\text{-}GAP}$ animals have abnormal functional connectivity between different cortical regions during specific brain states.

To record seizures, we previously performed 6-hr recordings utilizing skull-surface 32-channel EEG grids, as these mimic human high-density EEG recordings[18]. Here, we perform detailed analysis of the occurrence of multiple brain states during those recordings and find abnormalities in *Syngap*$^{+/\Delta\text{-}GAP}$ rats in the duration and number of sleep and wake occurrences during recordings, as well as differences in connectivity between cortical regions that may have value as clinically translatable biomarkers.

Materials and Methods

Animals

This paper uses data gathered during experiments for which some results have been previously published[17]. All animal procedures were undertaken in accordance with the University of Edinburgh animal welfare committee regulations and were performed under a UK Home Office project license. Long Evans-SG$^{em2/PWC}$, hereafter referred to as *Syngap*$^{+/\Delta\text{-}GAP}$ were kept on a 12h/12h light dark cycle with ad libitum access to water and food. Animals were genotyped by PCR. 12 *Syngap*$^{+/\Delta\text{-}GAP}$ and 12 *Syngap*$^{+/+}$ animals were recorded and used across all analyses.

Surgery

15 to 16 week-old *Syngap*$^{+/\Delta\text{-}GAP}$ and *Syngap*$^{+/+}$ male rates were anaesthetised with isoflurane and mounted on a stereotaxic frame. Two craniotomies were drilled for bilateral anchor screw placement (+4.0 mm AP, ± 0.5 mm ML) and one for ground screw implantation (-11.5 mm AP, 0.5 mm ML) (A2 Din M1x3 cheese head screw, Screwsandmore, UK), according to the frontal and caudal edges of the EEG array probe (H32-EEG – NeuroNexus, USA). The EEG probe was placed on the skull with its cross-symbol reference point aligned over bregma (Supplementary Fig. 1). The ground electrode and screw were connected with silver paint, and the implant was covered with dental cement. Animals were allowed to recover for a minimum of one-week post-surgery and were housed individually after surgery to prevent damage to the implant. Animals were monitored for any welfare issues arising during or after surgery as well as changes in behaviour, such as less food consumption or decreased responses to stimuli in cages, none were found.

EEG recordings

Prior to recording, rats were habituated for 20 to 30 minutes to the room. On recording days, up to 4 rats, were placed in individual side-by-side cages inside a 1 × 1 m faraday enclosure. Experimenters were blind to genotype. 6 hr EEG recordings, starting at zeitgeber time (ZT) 3 to 9 (under a 12 light hr: 12 dark hr schedule starting at 07:00 am) were acquired with an OpenEphys acquisition system (OpenEphys, Portugal), through individual 32-channel recording headstage amplifiers with accelerometers (RHD2132 Intantech, USA), at a sampling rate of 1 kHz.

Visual sleep scoring and absence seizure detection

Off-line visual brain state scoring blind to animal genotype was performed, assigning 5 s epochs to non rapid eye movement sleep (NREM), rapid eye movement sleep (REM) or wake. Scoring criteria for visual classification based was based on accelerometer and EEG characteristics[19,20]: NREM epochs displayed high-amplitude slow wave (~1 - 4 Hz) EEG activity accompanied by sleep spindles (~12 - 17 Hz) and decreased accelerometer activity. REM was identified by sustained theta (~5 - 10 Hz) and no accelerometer activity. Wake was identified by the presence of desynchronized EEG and varying levels of accelerometer activity.

We validated our accelerometer and EEG based visual scoring by comparing with recordings performed with electromyogram (EMG) and EEG. 4 *Syngap*$^{+/\Delta\text{-}GAP}$ and 4 *Syngap*$^{+/+}$ animals were surgically implanted with a 16-channel EEG surface probe array with 2 EMG leads (H16-Rat EEG16_Functional – NeuroNexus, MI, USA) implanted in neck muscles. Animals were recorded over five days for 24 hrs utilizing wireless headstages and an acquisition system (Tainitec, UK)[21]. Visual analysis was performed as described above utilizing EEG combined with EMG instead of accelerometer data over the 6 hours recorded in equivalent EEG accelerometer experiments at zeitgeber time 3 to 9 (under a 12 light hr: 12 dark hr schedule starting at 07:00 am. When comparing EEG-accelerometer and EEG-EMG modalities we

found no significant difference in percent time spent in wake (two-way ANOVA, F = 0.004, df = 1, p = 0.95, n= 12 *Syngap*$^{+/\Delta\text{-}GAP}$ and *Syngap*$^{+/+}$ EEG-accelerometer and n = 4 *Syngap*$^{+/\Delta\text{-}GAP}$ and *Syngap*$^{+/+}$ EEG-EMG, Supplementary Fig. 2A), NREM (two-way ANOVA, F = 0.079, df = 1, p = 0.472, n= 12 *Syngap*$^{+/\Delta\text{-}GAP}$ and *Syngap*$^{+/+}$ EEG-accelerometer and n = 4 *Syngap*$^{+/\Delta\text{-}GAP}$ and *Syngap*$^{+/+}$ EEG-EMG, Supplementary Fig. 2B) and REM (two-way ANOVA, F = 0.531, df = 1, p = 0.472, n= 12 *Syngap*$^{+/\Delta\text{-}GAP}$ and *Syngap*$^{+/+}$ EEG-accelerometer and n = 4 *Syngap*$^{+/\Delta\text{-}GAP}$ and *Syngap*$^{+/+}$ EEG-EMG, Supplementary Fig. 2C).

We previously quantified and reported the occurrence of absence seizures in *Syngap*$^{+/\Delta\text{-}GAP}$ rats[17] and excluded their occurrence times from our brain state analyses. The electrographical correlate of absence seizures, spike and wave discharges (SWDs), were identified visually and then analysis was confirmed with an automated absence seizure detection algorithm. Briefly, SWDs are characterized by periodic high amplitude oscillations in the theta band between 5 and 10 Hz[22] which correlates with a spontaneous stop in animal movement. Spectral analysis was performed that identified harmonic peaks in the power spectral density. The code used for analysis is available at https://github.com/Gonzalez-Sulser-Team/SWD-Automatic-Identification[17].

Automatic detection of sleep spindles

Automatic detection of sleep spindles during visually scored NREM sleep epochs was performed using the Matlab "Sleepwalker" toolbox with the "sw_run_delta_LFP.m" function (https://gitlab.com/ubartsch/sleepwalker)[23]. EEG signal from electrode placed over S1-Tr right were band-passed filtered between 12 - 17 Hz, with a minimum-maximum length between 0.2 - 3 s, a minimal time gap between events of 0.2 s, amplitude between 25 - 750 µV, a start to end limit threshold of 1.5 SD with a detection limit of 3 SD of the envelope and noise exclusion at ≥ 35 SD.

To detect spindles detected in multiple sites during NREM periods from electrodes that were less than 2 mm away from each other, we used the Python "Yasa" library function "spindles_detect" (https://zenodo.org/record/4632409) to identify spindles with a frequency range of 12 -17 Hz. The comparison was made specifically in electrodes that were within 2 mm distances from each other.

Spectral power and imaginary coherence analysis

Movement artefacts, identified visually as data points with values greater than 750 µV were discarded from further analysis. Spectral power for each individual epoch for all brain states (wake, NREM and REM) was calculated from an individual channel over the right primary somatosensory as the mean $\log_{10}$ power in the 0.2 - 48 Hz range (0.2 Hz steps) using the Multitaper package (Rahim, Burr & Thomson., 2014[5]) for R-studio (RStudio Team, 2020[6]). Epochs were then averaged per brain states for each individual animal.

For imaginary coherence averages across electrode pairs, the data were downsampled by a factor of 8 with the Python "Scipy.signal" function "decimate", which includes an order 8 Chebyshev type I filter for antialiasing, to increase processing speed. We calculated the coherence for each of the 32 pairs of electrodes in individual brains states in 99 frequency bins (1 – 50 Hz, 0.5 Hz bin size) with the Python Scipy "signal" function "coherence" and extracted the imaginary component using the Python Numpy function "imag"[24]. To ensure statistical normality, coherence values (R^2) from each 0.5 Hz frequency were *z*-transformed using Fisher's *r* to *z*, *z*-scores were then averaged at every 0.5 Hz bin and re-transformed

utilizing the Fisher inverse function to obtain the Z^{-1} coherence value per electrode pair and frequency band[25].

We calculated the Euclidean distance between all pairs of electrode using the Python SciPy "Spatial.distance" function "pdist", with 1.3 mm being the shortest distance between adjacent electrodes and 13.9 mm the longest distance electrode leads. We then utilized varying distance thresholds (from 2 - 10 mm in 1 mm increments) to compare imaginary coherence averages from short and long distances electrode pairs, between the groups of *Syngap*$^{+/\Delta\text{-}GAP}$ and *Syngap*$^{+/+}$ animals (Fig. 2A, Fig. 2D, Fig. 3G, Fig. 3A, Fig. 3D, Fig. 3G, and Supplementary Fig. 1 and Supplementary Fig. 3)[25].

Imaginary phase coherogram, representations of functional connectivity that depend on both frequency and time and are similar to a spectrograms, (Fig. 5A) were constructed during spindles using a complex Morlet wave convolution for 12-17 Hz using the "freqanalysis" function with the "wavelet" method from the Matlab Fieldtrip package. The wavelet cycle width was set to 7 with a length defined as 3 standard deviations (SDs) of the implicit Gaussian kernel. Connectivity analysis utilizing coherograms was performed using the "connectivityanalysis" function from the Matlab Fieldtrip package. Coherograms were averaged across specified channels over spindle occurrence times (500 ms preceding and 1500 ms following spindle start). Maximal imaginary coherence was identified over all coherogram time-frequency bins, 11 frequency components with 0.5 Hz steps from 12 to 17 Hz over 2000 time points for the 2000 ms was analysed, and used to quantify the number of time-frequency bins exceeding 70% of the maximum imaginary coherence.

Statistics

When normality and homoscedasticity were above the rejection value of < 0.05 (estimated by Shapiro–Wilk and Levene's tests respectively), between genotype comparisons across animals and electrodes were made with two-sample unpaired t-tests. Otherwise, a two-sample Mann Whitney-U rank sum test was used for unpaired two-sample comparison. Two-way ANOVAs were utilized to compare EEG-accelerometer with EEG-EMG brain state visual analyses, brain state power spectra and average Z' imaginary coherence in commonly used frequency bands. We utilized a non parametric two-sided permutation analysis with 40,000 simulation runs to compare average coherence per frequency band and over time during sleep spindles across electrode pairs. Consecutive significant frequencies clusters determined ranges with significant differences[26]. Person correlation, residuals, fit for testing relationship of SWDs with brain state abnormalities and imaginary coherence differences.

In this study we analysed data recorded from *Syngap*$^{+/\Delta\text{-}GAP}$ and *Syngap*$^{+/+}$, which previously allowed us to show significant differences in the incidence and duration of absence seizures[17]. For our a priori statistical power calculations for the present study we utilized alpha = 0.05. For comparisons between genotypes of percent time, total minutes and average duration of individual brain state bouts we estimated based on changes in brain states in mutant mice from similar results reported in another neurodevelopmental model[27]. For total minutes we set the mean of the control to 75 min, the mean of the mutant group to 55 min and the standard deviation for the mutants was 15.8. For n = 12 the resulting power is 0.803 and effect size 1.27.

Data Availability

Upon article acceptance data will be made freely available on OpenNeuro (https://openneuro.org/) and can be obtained directly from the corresponding author.

Funding
The work performed here was funded by The Simons Initiative for the Developing Brain, the Patrick Wild Centre, an Epilepsy Research United Kingdom grant [F1603] and a Wellcome Trust Institutional Support Fund grant [204804/Z/16/Z]. For the purpose of open access, the author has applied a CC BY public copyright licence to any Author Accepted Manuscript version arising from this submission.

Author Contributions
P.C.K., J.E., S.M.T. and A.G-S. designed the experiments. I.B.P. performed the experiments. I.B-P., J.M-R. and Z. L. analysed the data. A.G-S. wrote the manuscript with input from all authors.

Competing Interests
The authors report no competing interests.

Results

Sleep-wake distribution and spectral properties in *Syngap*$^{+/\Delta\text{-}GAP}$ rats

We previously reported that Syngap$^{+/\Delta\text{-}GAP}$ rats displayed absence seizures more frequently than littermate controls utilizing six-hour EEG (Fig. 1A, Supplementary Fig. 1) recordings when animals were in a quiet-wake state[17]. To determine whether *Syngap*$^{+/\Delta\text{-}GAP}$ animals have abnormalities in their brain state distribution, we classified all individual 5 s recording epochs from those previous recordings as NREM sleep, REM sleep or wake (Fig. 1A).

We found that *Syngap*$^{+/\Delta\text{-}GAP}$ rats spent an equivalent percentage of time in all states when compared to wild-type littermate controls (unpaired two-sample t-test for REM: DF = 22, T = 0.67, p=0.51; NREM: DF = 22, T = 0.0025, p = 0.1; wake: DF = 22, T = 0.26, p=0.8; Fig. 1B-D). Nonetheless, *Syngap*$^{+/\Delta\text{-}GAP}$ animals had a significantly lower number of wake and NREM bouts, with REM bouts remaining unchanged (unpaired two-sample t-test for REM: DF = 22, T = 0.21, p=0.83; wake: DF = 22, T = 3.8, p= 0.00095; NREM sleep: DF = 22, T = =3.5, p=0.002; Fig. 1B-D). This coincided with increased average bout duration during wake and NREM and, no-difference in REM bout duration (unpaired two-sample t-test for REM: DF = 22, T = 0.79, p=0.44; wake: DF = 22, T = 2.57, p=0.017; two-sample Mann Whitney-U rank sum test for NREM: U=25, p=0.007, Fig. 1B-D). Therefore, during 6 hr recordings, *Syngap*$^{+/\Delta\text{-}GAP}$ rats display an abnormal brain state distribution.

We calculated the average EEG spectral power from one representative channel across all animals and epochs of each brain state and found no significant differences between *Syngap*$^{+/\Delta\text{-}GAP}$ rats and their wild-type littermates in commonly utilized frequency bands during NREM (two-way ANOVA, p = 0.60, F = 0.27, df = 1; Fig. 1E and H), REM (two-way ANOVA, p = 0.68, F = 0.17, df = 1; Fig. 1F and I) or wake (two-way ANOVA, p = 0.60, F = 0.27, df = 1; Fig. 1E and H), REM (two-way ANOVA, p = 0.76, F = 0.09, df = 1; Fig. 1G and Fig. 1J). These data show that *Syngap*$^{+/\Delta\text{-}GAP}$ rats display an abnormal sleep-wake distribution, although overall spectral properties across all frequency bands were unchanged.

Functional connectivity in *Syngap*$^{+/\Delta\text{-}GAP}$ rats

Abnormalities in synaptic connectivity may underlie the cognitive pathologies and epilepsy in *SYNGAP* haploinsufficiency[28,29]. Network activity pathophysiology in neurodevelopmental disorders may be detected by analysing connectivity between EEG electrodes[30]. We therefore analysed the imaginary coherence, a generalization of correlation in the phase domain[24], between voltage signals in our multi-site recordings during each brain state. Imaginary coherence decreases the likelihood of false dependencies between electrodes due to volume conductance by correlating between signal phases and not amplitude. We calculated the imaginary coherence for frequencies from 0 to 50 Hz for each brain state averaged across all

epochs for all 496 combinations of electrode pairs from the 32 electrodes recorded. Since short or long distance connections may be differentially affected in neurodevelopmental disorders and may display varying levels of correlation[25], imaginary coherence values were then averaged by electrodes that were grouped by short or long distances (Fig. 2, Fig. 3, Supplementary Fig. 1 and Supplementary Fig. 3).

As rodent surface multi-site EEG probes have not been previously utilized to compare short and long-distance electrode connectivity, we calculated whether there were differences between *Syngap*$^{+/\Delta\text{-}GAP}$ rats and wild-type controls using multiple distance thresholds separating groups of channels into short and long-distance channel combinations (Fig. 2, Fig. 3 and Supplementary Fig. 3). The most striking differences occurred during NREM amongst short-distance pairs < 2 mm from each other (Fig. 2A, Fig. 2B, Fig. 2C and Supplementary Fig. 3). When comparing commonly used frequency bands there was a clear, although none significant, trend towards decreased theta and sigma band imaginary coherence in *Syngap*$^{+/\Delta\text{-}GAP}$ rats (two-way ANOVA, $p = 0.06$, $F = 3.54$, $df = 1$, Fig. 2A and Fig. 2B). To identify abnormal frequency bands, we utilized an unbiased approach in which we compared the imaginary coherence between the two groups by statistically testing each individual 0.5 Hz frequency bin between 0.5 and 50 Hz and plotting p-values as a function of frequency[26]. We found clusters of consecutive significantly different frequencies with $p \leq 0.05$ corresponding to frequencies with significantly decreased *Syngap*$^{+/\Delta\text{-}GAP}$ imaginary coherence (two-sided randomization based none parametric test with cluster-based multiple comparison correction, Fig. 2C). These clusters occurred between 5 and 9 Hz and between 11.5 and 29.5 Hz. Furthermore, there was a striking subset of consecutive frequencies with lower p-values ($p \leq 0.01$) between 12 and 22 Hz (Fig. 2C and Supplementary Fig. 3B). That range overlaps with the reported frequency range of sleep spindles (12 to 17 Hz), which are characteristic of NREM sleep and are thought to be critical for normal brain function and memory consolidation[31,32]. This cluster of significantly lower imaginary coherence frequencies suggests that connectivity may be compromised specifically during sleep spindles in *Syngap*$^{+/\Delta\text{-}GAP}$ animals in short-range distance electrode pairs.

There were no significant differences in commonly utilized frequency bands in short-distance electrodes < 2 mm during REM (two-way ANOVA, $p = 0.75$, $F = 0.10$, $df = 1$, Fig. 2D and Fig. 2E) although a trend towards significance in the sigma band was evident in wake periods (two-way ANOVA, $p = 0.10$, $F = 2.72$, $df = 1$, Fig. 2G, H). In contrast to NREM, there was only a small cluster of frequencies between 16 and 18 Hz during REM with $p \leq 0.05$ (two-sided randomization based none parametric test with cluster-based multiple comparison correction, Fig. 2F). While in wake there were no significantly different frequencies (two-sided randomization based none parametric test with cluster-based multiple comparison correction, Fig. 2I).

We also compared electrode pairs > 2 mm from each other as long-distance connectivity has been shown to be increased in children with other neurodevelopmental disorders[25]. There were no significant differences in standard frequency bands between genotypes during NREM (two-way ANOVA, $p = 0.57$, $F = 0.33$, $df = 1$, Fig. 3A and Fig. 3B) or REM (two-way ANOVA, $p = 0.76$, $F = 0.09$, $df = 1$, Fig. 3E and Fig. 3F). This was confirmed by a lack of significantly different frequency clusters in both NREM and REM (two-sided randomization based none parametric test with cluster-based multiple comparison correction, Fig. 3C and Fig. 3F). However, a distinct none significant trend towards increased theta and sigma coherence in *Syngap*$^{+/\Delta\text{-}GAP}$ rats during wake in long distance electrode pairs was detected (two-way ANOVA, $p = 0.06$, $F = 3.72$, $df = 1$, Fig. 3G and Fig. 3H). Clusters of consecutive significant frequencies, with $p \leq 0.05$ showing higher connectivity in *Syngap*$^{+/\Delta\text{-}GAP}$ rats, were present during wake in the theta range between 8 and 9.5 Hz, and in the sigma range between 14 and 16.5 Hz (two-sided randomization based none parametric test with cluster-based multiple comparison correction, Fig. 3I), suggesting hyper-connectivity phenotypes may be present during wake in *Syngap*$^{+/\Delta\text{-}GAP}$ rats.

Since short-distance electrode pairs had abnormalities in functional connectivity in *Syngap*$^{+/\Delta\text{-}GAP}$ we posited that cortical regions may have compromised imaginary coherence between each other. We tested whether specific cortical areas had disruptions in functional connectivity by averaging voltage signals from channels in three rostral to caudal bilateral regions (Supplementary Fig. 4A) and calculating the imaginary coherence between regions during NREM, as our primary abnormality was in the 11.5 to 29.5 frequency range in that brain state. However, we found no clusters of significant values in any comparison between regions (Supplementary Fig. 4B), suggesting that the abnormality in NREM is specific to short-distance channels.

Overall, these data show that *Syngap*$^{+/\Delta\text{-}GAP}$ rats have connectivity abnormalities between electrode pairs located at varying distances from each other, with particularly striking deficiencies in imaginary coherence during NREM amongst short-distance pairs of electrodes. Electrodes < 2 mm from each other mainly correspond to pairs of electrodes overlaying cortical areas with equivalent functionality, such as visual, motor or somatosensory areas (Fig 2A and Supplementary Fig. 1), suggesting that imaginary coherence abnormalities occur in local connections within cortical regions with a defined function.

SWDs and brain state abnormalities in *Syngap*$^{+/\Delta\text{-}GAP}$ rats

A critical question in epileptic encephalopathies such as SYNGAP1 haploinsufficiency is whether the presence of seizures influences other neurodevelopmental phenotypes. We previously reported that SWDs (Fig. 4A), the electrophysiological correlate of absence seizures, are significantly more prevalent in Syngap$^{+/\Delta\text{-}GAP}$ rats than in littermate controls[17]. We hypothesized that SWDs may correlate with time spent in specific brain states as well as cortical connectivity. We tested whether the percentage amount of time spent in SWDs was correlated to sleep abnormalities (Fig. 1C, D) and the average imaginary coherence values during NREM in the frequency range between 12 and 22 Hz where there were connectivity deficits with low p-values ($p \leq 0.01$) (Fig 2A, C). SWDs in Syngap$^{+/\Delta\text{-}GAP}$ rats were not significantly correlated to number of NREM bouts (Pearson correlation, DF = 1, F = 0.511, R = -0.22, p = 0.491, Fig 4B), average NREM bout duration (Pearson correlation, DF = 1, F = 0.803, R = -0.273, p = 0.391, Fig 4C), or number of wake bouts (Pearson correlation, DF = 1, F = 0.766, R = -0.267, p = 0.402, Fig 4D). SWDs were significantly correlated to average wake bout duration (Pearson correlation, DF = 1, F = 9.833, R = 0.704, p = 0.0106, Fig 4E). However, we found no significant correlation between SWD time and the primary average imaginary coherence difference recorded in the 12 – 22 Hz frequency range during NREM (Pearson correlation, DF = 1, F = 0.429, R = -0.203, p = 0.527, Fig 4F). Only average wake bout duration correlates with SWDs, suggesting that absence seizures only minimally affect sleep and connectivity abnormalities.

Sleep spindles in *Syngap*$^{+/\Delta\text{-}GAP}$ rats

Due to the reduction in average imaginary coherence in the sleep spindle frequency range in short-distance electrode combinations, we assessed whether sleep spindles were abnormal in *Syngap*$^{+/\Delta\text{-}GAP}$ rats (Fig. 5A). We first automatically detected spindles across animals from a single channel, over the right primary somatosensory cortex (Supplementary Fig. 1), to determine whether spindle number and duration is altered in *Syngap*$^{+/\Delta\text{-}GAP}$ rats. There was no significant difference in the total number of spindles detected (two-sample unpaired t-test, DF = 22, T = 0.59, p = 0.56, Fig. 5B) although there was a small decrease in the average duration of spindles in *Syngap*$^{+/\Delta\text{-}GAP}$ rats when compared to wild-type littermates (two-sample unpaired t-test, DF = 22, T = 2.19, p = 0.039, Fig. 5C). The average spindle amplitude was not significantly different between both genotypes (two-sample unpaired t-test, DF = 22, T = 0.75,

p = 0.461, Fig. 5D) nor was the average power after spindle detection in the 12 to 17 Hz band (Mann-Whitney u-test, U = 52, p = 0.26, Fig. 5E). We then automatically detected spindles across all channels during NREM to assess whether there was a deficit between how spindles spread between short-distance pairs of electrodes. We found that there was no significant difference between *Syngap*$^{+/\Delta\text{-}GAP}$ rats and wild-type littermates in both the number of times that a spindle was simultaneously identified in more than one electrode (two-sample unpaired t-test, DF = 22, T = 1.78, p=0.26 Fig. 5F) and the number of electrodes in which a spindle was present when it was detected in more than one electrode (two-sample unpaired t-test, DF = 22, T = -0.92, p=0.37, Fig. 5G). These results show that spindle occurrence, amplitude, spectral power and detection of spindles throughout the cortex are unchanged in *Syngap*$^{+/\Delta\text{-}GAP}$ rats.

Dynamic functional connectivity in *Syngap*$^{+/\Delta\text{-}GAP}$ rats during sleep spindles

We hypothesized that the significant reduction in average imaginary coherence in *Syngap*$^{+/\Delta\text{-}GAP}$ rats during NREM in short-distance electrode pairs may be a consequence of deficits in connectivity across channels during spindles. We therefore calculated average imaginary coherograms during spindles across all electrode combinations at distances ≤ 2 mm from each other for each animal, and we identified the total number of time-frequency bins in the coherograms that exceeded 70 % of the maximum connectivity detected in each individual animal (Fig. 5A). We found that *Syngap*$^{+/\Delta\text{-}GAP}$ rats had significantly decreased total high connectivity time-frequency bins from average coherograms when compared to wild-type controls (two-sample unpaired t-test, DF = 22, T = -2.39, p=0.03, Fig. 6B). This coincided with a significant increase in the spectral frequency at which high-connectivity time-frequency bins occurred (two-sample unpaired t-test, DF = 22, T = 2.13, p=0.04, Fig. 6C). These data show that there is a deficit in the occurrences of high functional connectivity in *Syngap*$^{+/\Delta\text{-}GAP}$ rats during spindles that may contribute to the overall decrease in imaginary coherence during NREM amongst short-distance electrode pairs.

We also compared the average values of imaginary coherence from coherograms during the entire length of spindles between the two genotypes and found that there was no significant reduction both across averages from all 496 channel combinations (two-sample unpaired t-test, DF = 22, T = 1.34, p = 0.19, Fig. 7B) and across averages from pairs of channels ≤ 2 mm from each other (two-sample unpaired t-test, DF = 22, T = 1.72, p = 0.10, Fig. 7B). This suggests that what contributes to decreased spindle coherence in short-distance channels is the reduction of occurrences of high-connectivity during spindles and not the overall average across the entire 12 to 17 Hz range and time preceding and following the start of spindles.

It is possible that specific channel combinations that are not organized by distance but by cortical location may have altered coherence during spindles. We therefore analysed whether specific channel pairs had significantly decreased connectivity when compared across animals and we found 45 combinations of channels where the imaginary coherence was significantly decreased in *Syngap*$^{+/\Delta\text{-}GAP}$ rats between 12 and 17 Hz (Fig. 6A and Supplementary Table 1). These channels were located caudal to bregma predominantly on the right posterior hemisphere over somatosensory, association and visual cortices (Fig. 6A and Supplementary Fig. 1). Some long-range and interhemispheric channel pairs also showed differences between the groups (Fig. 7A). When we evaluated the average imaginary coherence for these channel combinations, we found a significant decrease in *Syngap*$^{+/\Delta\text{-}GAP}$ rats compared to controls (two-sample unpaired t-test, DF = 22, T = 3.04, p = 0.006, Fig. 7B). This was confirmed by comparing specific time points before and during spindles between the two genotypes utilizing the different combinations of electrode pairs. Clear and long clusters of consecutively significant timepoints, p ≤ 0.05, were present when utilizing the 45 channels with significantly decreased coherence and not when utilizing all 496 pairs or electrodes < 2

mm from each other (two-sided randomization based none parametric test with cluster-based multiple comparison correction, Fig. 7C).

We then tested whether specific cortical areas had significant differences in dynamic connectivity during spindles. Voltages during all spindles were averaged across channels in specific regions (Fig. 7D) and dynamic imaginary coherence was calculated between regional pairs (Fig. 7E, Supplementary Fig. 4). Long clusters of significantly different time points during spindles were only found in regional pairs in the right middle - left middle, right middle - right caudal and left middle - right caudal - regional pairs (Fig 7E), which are regions that overlap with the 45 channel pairs identified that had significantly decreased connectivity (Fig 7A). The three regional pairs had long clusters of timepoints in which the imaginary coherence was significantly decreased *Syngap*$^{+/\Delta\text{-}GAP}$ rats at approximately 500 ms, which corresponds to the start of the spindle (two-sided randomization based none parametric test with cluster-based multiple comparison correction, right middle - left middle between 497 and 567 ms, right middle - right caudal between 466 and 754 ms, left middle - right caudal 490 and 545 ms). In the right middle - right caudal and left middle - right caudal regional pairs, there were a second cluster of significant times after approximately 1000 ms (two-sided randomization based none parametric test with cluster-based multiple comparison correction, right middle - right caudal between 1045 and 1093 ms, left middle - right caudal 1077 and 1087 ms) and 1500 ms (two-sided randomization based none parametric test with cluster-based multiple comparison correction, right middle - right caudal between 1525 and 1627 ms, left middle - right caudal 1529 and 1584 ms). This indicates that the imaginary coherence between specific sets of regional and channel connections is significantly reduced during sleep spindles in *Syngap*$^{+/\Delta\text{-}GAP}$ rats compared to wild-type controls.

Overall, these results show that there are deficits in instances of high functional connectivity during spindles amongst electrode combinations at short distances from each other, while a subset of electrode combinations and regions have a higher degree of connectivity deficit suggesting potential deficits in *Syngap*$^{+/\Delta\text{-}GAP}$ rats in specific underlying cortical anatomy.

Discussion

We show that brain states are altered in *Syngap*$^{+/\Delta\text{-}GAP}$ animals as the number of NREM and wake bouts are decreased. Nonetheless a corresponding increase in average NREM and wake bout duration in *Syngap*$^{+/\Delta\text{-}GAP}$ rats resulted in an equal percentage of time spent in NREM, REM and wake states when compared to wild type controls. Although no significant differences in spectral power or imaginary coherence were detected in commonly utilized frequency bands; when imagery coherence was compared between genotypes with a none biased none parametric method, clear decreases in *Syngap*$^{+/\Delta\text{-}GAP}$ animals in electrode pairs < 2 mm apart during NREM between 11.5 and 29.5 Hz were present. The overlap of the decrease in imaginary coherence during NREM with the sleep spindle frequency range amongst pairs of electrodes < 2 mm apart, prompted an in-depth analysis in sleep spindle properties. The occurrence, amplitude, power and detection of sleep spindles across multiple electrodes was unchanged in *Syngap*$^{+/\Delta\text{-}GAP}$ rats with only a small decrease in duration detected. Notwithstanding, dynamic coherence analysis revealed that during spindles, instances of high connectivity were decreased in *Syngap*$^{+/\Delta\text{-}GAP}$ animals, which was accompanied by an increase in average high-connectivity imaginary coherence frequency. Finally, the average coherence during spindles amongst all pairs of electrodes, as well as those < 2 mm apart, was not significantly different between genotypes despite the decrease in the instances of high connectivity for electrodes < 2mm in *Syngap*$^{+/\Delta\text{-}GAP}$ rats. However, by identifying a subset of electrodes with significantly decreased connectivity during spindles in *Syngap*$^{+/\Delta\text{-}GAP}$ animals, we found that as a group, these electrodes did show average decreased connectivity. These electrodes were primarily located in the right caudal hemisphere, suggesting that cortical dynamics at this location may be particularly affected by the *SYNGAP1* mutation.

Absence seizures are the most prevalent seizure type in *SYNGAP1* haploinsufficiency patients, with 53/57 cases having absence seizures in a recent clinical report[3]. *Syngap*$^{+/\Delta\text{-}GAP}$ are to our knowledge, the only pre-clinical model of *SYNGAP1* with spontaneous absence seizures[17]. Replication of such an important phenotype suggests that this model has a high face validity and therefore biomarkers identified here may have particular translational relevance.

The percent recording time spent in SWDs was positively correlated with wake bout duration, but it was not correlated with the number of NREM bouts or their duration, the number of wake bouts or imaginary coherence values between electrodes < 2 mm apart during spindles in *Syngap*$^{+/\Delta\text{-}GAP}$. These data suggest that deletion of the C2 and GAP domains of *SYNGAP1* may result in independent circuit mechanisms leading to sleep and connectivity deficits and seizures.

Difficulties in both initiating and maintaining sleep as well as reduced overall sleep duration have been reported in individuals with *SYNGAP1* mutations[3,8,9]. In our previous work we performed 6 hr recordings EEG recordings and found that *Syngap*$^{+/\Delta\text{-}GAP}$ animals displayed absence seizures at a higher rate than controls [17]. We have further analysed these recordings, which were made during daylight hours, resulting in rats spending approximately half of the recording time asleep. Despite recent clinical reports, we found that the overall time spent asleep was not different from littermate controls in mutant animals. Nonetheless, the number of times that *Syngap*$^{+/\Delta\text{-}GAP}$ rats entered NREM or wake brain states was decreased. Interestingly, there was also an increase in the duration of NREM and wake bouts, which suggest that overall sleep structure is compromised in these animals. Since sleep is intermingled with wake states throughout the day in rats, full-day circadian recordings may identify further sleep abnormalities in this mutant line.

EEG has been suggested as a potential method to identify clinical biomarkers in NDDs [33] and indeed analysis of EEG connectivity and networks have yielded specific signatures for epilepsy and autism[25,34]. For example, in temporal lobe epilepsy, high frequency oscillations recorded with intracranial EEG can be utilized to identify the seizure onset zone and improve the efficacy of surgical brain resection to control seizures[35]. Furthermore, it has been proposed that analysing the spatiotemporal coherence of high frequency oscillations can yield more spatially refined targeting of the seizure onset zone[36]. Modifying network oscillatory rhythms has proven effective in curtailing seizures in rodent models of temporal lobe epilepsy[37], and may be an important mechanistic component of how deep brain stimulation of the anterior nucleus of the thalamus controls seizures in patients[38]. In tuberous sclerosis complex EEG coherence abnormalities in infants are associated with the development of autism spectrum disorders[39], while a high level of EEG mutual information, another metric of connectivity, predicts the emergence of epileptic spasms[40]. In patients with Lennox Gastaut syndrome and Dravet syndrome, severe epileptic encephalopathies with refractory seizures, abnormalities in phase coherence and graph theory metrics predict the effectiveness of cannabidiol treatment.[41]

Similarly to human EEG, it may be that abnormalities present in brain circuit activity are only detectable through intracranial recordings, such as with high frequency oscillations in temporal lobe epilepsy, which are reduced in duration and amplitude in surface recordings[42], with higher frequency oscillations being more vulnerable to skull and skin tissue interference[43], which is why we focused our analysis on frequencies lower than 50 Hz.

Here, we performed analysis on the connectivity between electrode pairs from our multi-site EEG probes. We utilized imaginary coherence since the likelihood of volume conductance artefacts with a method analysing amplitude correlations, may be higher with the reduced skull size of rats compared to humans.

We separated electrode pairs between short and long distance groups and averaged the overall coherence within these groups. We performed comparisons with varying threshold distances separating short and long distance electrode pair groups and found that the clearest deficits in connectivity in *Syngap*$^{+/\Delta\text{-}GAP}$ rats occurred during NREM in short distance electrodes < 2 mm. SYNGAP is primarily located in excitatory synapses and is a key regulator of spine formation[14–16]. Cortical pyramidal cells form most of their intracortical connections with neighbours in close proximity[44]. Electrodes with < 2 mm distance from each other are mainly located over cortical areas with similar function such as motor, visual or somatosensory processing (Fig 2A and Supplementary Fig. 1). These data suggest that in *SYNGAP1* haploinsufficiency human patients there may be a deficit in connections within regions of cortex with a common function, which may be heightened during cortical activity in NREM.

Across brain states there were no significant differences in power, although there was a reduction in imaginary coherence between short distance electrodes during NREM and an increase in imaginary coherence between long distance electrodes during wake. Imaginary coherence has been proposed as a method to more accurately measure the interactions between brain regions[24]. Power at an individual channel can be independent of the coherence measured between that channel and another. In fact, in recent work in Angelman syndrome patients, abnormalities in power at specific bands are not necessarily reflected in coherence calculations, and vice versa, coherence abnormalities are often associated with no changes in power[12,25].

One of the characteristics of NREM are sleep spindles, which are thought to be critical for memory processes[32], and lower imaginary coherence in the spindle frequency range led us to investigate their characteristics in *Syngap*$^{+/\Delta\text{-}GAP}$ animals. We found that their overall characteristics were unaffected, as well as the average connectivity during a spindle. Nonetheless, brief periods of high connectivity were significantly decreased in *Syngap*$^{+/\Delta\text{-}GAP}$ rats, with a concurrent increase in the oscillatory frequency at which these high connectivity events occurred. How cortical neuronal populations interact during sleep spindles may be compromised in *Syngap*$^{+/\Delta\text{-}GAP}$ animals. Analysis of sleep spindle connectivity between individual channel combinations showed that a subgroup of connections had significantly lower imaginary coherence in *Syngap*$^{+/\Delta\text{-}GAP}$ rats. This area is located over the right somatosensory, association and visual cortices, which may be more vulnerable to deficits due to *SYNGAP1* mutation. Some interhemispheric connectivity abnormalities may also be present, although the overall average imaginary coherence between long-distance connections was not significantly altered during NREM (Fig. 3C). Nonetheless, when we compared dynamic imaginary coherence by specific cortical regions (Fig 7D, E), we found that these overlapped with significantly different channel combinations. The locations with significant decreases in connectivity were located between the left middle cortical area and the contralateral middle and caudal regions. There was also a deficit between the middle and caudal areas over the right hemisphere. These data suggest that these regions may be specifically affected in *Syngap*$^{+/\Delta\text{-}GAP}$ rats.

Finally, we saw that despite decreases in the overall number of NREM and wake bouts, the overall time spent in those states was not decreased due to their increased duration in *Syngap*$^{+/\Delta\text{-}GAP}$ animals. Interestingly, we also saw decreased connectivity during NREM in the sigma range in mutant animals, which was accompanied by increased connectivity in the theta and sigma range during wake. A degree of homeostatic adaptation may be occurring in mutant animals to counteract the effects of the mutation during different brain states.

In conclusion, we report sleep abnormalities and differences in connectivity during specific brain states in the *Syngap*$^{+/\Delta\text{-}GAP}$ rat model. Imaginary coherence analysis of EEG data may have value as a clinical biomarker and this analysis points to specific neuronal populations that may be affected by the mutation.

References

1. Parikshak NN, Luo R, Zhang A, et al. Integrative Functional Genomic Analyses Implicate Specific Molecular Pathways and Circuits in Autism. *Cell*. 2013;155(5):1008-1021. doi:10.1016/j.cell.2013.10.031
2. Hamdan FF, Gauthier J, Spiegelman D, et al. Mutations in SYNGAP1 in Autosomal Nonsyndromic Mental Retardation F. *N Engl J Med*. 2009;360(6):599-605.
3. Vlaskamp DRM, Shaw BJ, Burgess R, et al. SYNGAP1 encephalopathy: A distinctive generalized developmental and epileptic encephalopathy. *Neurology*. 2019;92(2):E96-E107. doi:10.1212/WNL.0000000000006729
4. Deciphering Developmental Disorders. Europe PMC Funders Group Large-scale discovery of novel genetic causes of developmental disorders. 2015;519(7542):223-228. doi:10.1038/nature14135.Large-scale
5. Deciphering Developmental Disorders. Prevalence and architecture of de novo mutations in developmental disorders. *Nature*. 2017;542(7642):433-438. doi:10.1038/nature21062
6. Satterstrom FK, Kosmicki JA, Wang J, et al. Large-Scale Exome Sequencing Study Implicates Both Developmental and Functional Changes in the Neurobiology of Autism. *Cell*. 2020;180(3):568-584.e23. doi:10.1016/j.cell.2019.12.036
7. Carvill GL, Heavin SB, Yendle SC, et al. Targeted resequencing in epileptic encephalopathies identifies de novo mutations in CHD2 and SYNGAP1. *Nat Publ Gr*. 2013;45(7). doi:10.1038/ng.2646
8. Jimenez-Gomez A, Niu S, Andujar-Perez F, et al. Phenotypic characterization of individuals with SYNGAP1 pathogenic variants reveals a potential correlation between posterior dominant rhythm and developmental progression. *J Neurodev Disord*. 2019;11(1):1-11. doi:10.1186/s11689-019-9276-y
9. Smith-Hicks C, Wright D, Kenny A, et al. Sleep abnormalities in the synaptopathies—syngap1-related intellectual disability and phelan–mcdermid syndrome. *Brain Sci*. 2021;11(9):1-10. doi:10.3390/brainsci11091229
10. Sahin M, Jones SR, Sweeney JA, et al. Discovering translational biomarkers in neurodevelopmental disorders. *Nat Rev Drug Discov*. 2019;18(april):235-236. doi:10.1038/d41573-018-00010-7
11. Lau-zhu A, Lau MPH, Mcloughlin G. Developmental Cognitive Neuroscience Mobile EEG in research on neurodevelopmental disorders : Opportunities and challenges. *Dev Cogn Neurosci*. 2019;36(March):100635. doi:10.1016/j.dcn.2019.100635
12. Sidorov MS, Deck GM, Dolatshahi M, et al. Delta rhythmicity is a reliable EEG biomarker in Angelman syndrome: A parallel mouse and human analysis. *J Neurodev Disord*. 2017;9(1):1-14. doi:10.1186/s11689-017-9195-8
13. Lopez-Rivera JA, Perez-Palma E, Symonds J, et al. A catalogue of new incidence estimates of monogenic neurodevelopmental disorders caused by de novo variants. *Brain*. 2020;143:1099-1105. doi:10.1093/brain/awaa051
14. Chen HJ, Rojas-Soto M, Oguni A, Kennedy MB. A synaptic Ras-GTPase activating protein (p135 SynGAP) inhibited by CaM kinase II. *Neuron*. 1998;20(5):895-904. doi:10.1016/S0896-6273(00)80471-7
15. Kim JH, Liao D, Lau LF, Huganir RL. SynGAP: A synaptic RasGAP that associates with the PSD-95/SAP90 protein family. *Neuron*. 1998;20(4):683-691. doi:10.1016/S0896-6273(00)81008-9
16. Gamache TR, Araki Y, Huganir RL. Twenty years of syngap research: From synapses to cognition. *J Neurosci*. 2020;40(8):1596-1605. doi:10.1523/JNEUROSCI.0420-19.2020
17. Katsanevaki D, Till MS, Buller-Peralta I, et al. Heterozygous deletion of SYNGAP enzymatic domains in rats causes selective learning, social and seizure phenotypes. *bioRxiv*. Published online 2020. doi:2020.10.14.339192
18. Jonak CR, Lovelace JW, Ethell IM, Razak KA, Binder DK. Multielectrode array

analysis of EEG biomarkers in a mouse model of Fragile X Syndrome. *Neurobiol Dis*. 2020;138(November 2019):104794. doi:10.1016/j.nbd.2020.104794

19. Lampert T, Plano A, Austin J, Platt B. On the identification of sleep stages in mouse electroencephalography. *J Neurosci Methods*. 2015;246:52-64. doi:10.1016/j.jneumeth.2015.03.007
20. Mondino A, Cavelli M, González J, et al. Power and Coherence in the EEG of the Rat: Impact of Behavioral States, Cortical Area, Lateralization and Light/Dark Phases. *Clocks & Sleep*. 2020;2(4):536-556. doi:10.3390/clockssleep2040039
21. Jiang Z, Huxter JR, Bowyer SA, et al. TaiNi: Maximizing research output whilst improving animals' welfare in neurophysiology experiments. *Sci Rep*. 2017;7(1):1-12. doi:10.1038/s41598-017-08078-8
22. Crunelli V, Lőrincz ML, McCafferty C, et al. Clinical and experimental insight into pathophysiology, comorbidity and therapy of absence seizures. *Brain*. 2020;(May). doi:10.1093/brain/awaa072
23. Bartsch U, Simpkin AJ, Demanuele C, Wamsley E, Marston HM, Jones MW. Distributed slow-wave dynamics during sleep predict memory consolidation and its impairment in schizophrenia. *npj Schizophr*. 2019;5(1):1-11. doi:10.1038/s41537-019-0086-8
24. Nolte G, Bai O, Wheaton L, Mari Z, Vorbach S, Hallett M. Identifying true brain interaction from EEG data using the imaginary part of coherency. *Clin Neurophysiol*. 2004;115:2292-2307. doi:10.1016/j.clinph.2004.04.029
25. Den Bakker H, Sidorov MS, Fan Z, et al. Abnormal coherence and sleep composition in children with Angelman syndrome: A retrospective EEG study. *Mol Autism*. 2018;9(1):1-12. doi:10.1186/s13229-018-0214-8
26. Maris E, Oostenveld R. Nonparametric statistical testing of EEG- and MEG-data. *J Neurosci Methods*. 2007;164(1):177-190. doi:10.1016/j.jneumeth.2007.03.024
27. Ingiosi A, Schoch H, Wintler TP, et al. Shank3 Modulates Sleep and Expression of Circadian Transcription Factors. *Elife*. 2019;8:1-23. doi:10.7554/elife.42819
28. Aceti M, Creson TK, Vaissiere T, et al. Syngap1 haploinsufficiency damages a postnatal critical period of pyramidal cell structural maturation linked to cortical circuit assembly. *Biol Psychiatry*. 2015;77(9):805-815. doi:10.1016/j.biopsych.2014.08.001
29. Berryer MH, Chattopadhyaya B, Xing P, et al. Decrease of SYNGAP1 in GABAergic cells impairs inhibitory synapse connectivity, synaptic inhibition and cognitive function. *Nat Commun*. 2016;7. doi:10.1038/ncomms13340
30. Bosl WJ, Tager-flusberg H, Nelson CA. EEG Analytics for Early Detection of Autism Spectrum Disorder : A data-driven approach. *Sci Rep*. Published online 2018:1-20. doi:10.1038/s41598-018-24318-x
31. Van Luijtelaar ELJM. Spike-wave discharges and sleep spindles in rats. *Acta Neurobiol Exp (Wars)*. 1997;57(2):113-121.
32. Lüthi A. Sleep Spindles : Where They Come From , What They Do. *Neuroscientist*. 2014;20(3):243-256. doi:10.1177/1073858413500854
33. Bosl W, Tierney A, Tager-Flusberg H, Nelson C. EEG complexity as a biomarker for autism spectrum disorder risk. *BMC Med*. 2011;9. doi:10.1186/1741-7015-9-18
34. Kinney-Lang E, Yoong M, Hunter M, et al. Analysis of EEG networks and their correlation with cognitive impairment in preschool children with epilepsy. *Epilepsy Behav*. 2019;90:45-56. doi:10.1016/j.yebeh.2018.11.011
35. Akiyama T, McCoy B, Go CY, et al. Focal resection of fast ripples on extraoperative intracranial EEG improves seizure outcome in pediatric epilepsy. *Epilepsia*. 2011;52(10):1802-1811. doi:10.1111/j.1528-1167.2011.03199.x
36. Cotic M, Zalay OC, Chinvarun Y, Del Campo M, Carlen PL, Bardakjian BL. Mapping the coherence of ictal high frequency oscillations in human extratemporal lobe epilepsy. *Epilepsia*. 2015;56(3):393-402. doi:10.1111/epi.12918
37. Hristova K, Martinez-gonzalez C, Watson TC, et al. Medial septal GABAergic neurons reduce seizure duration upon optogenetic closed-loop stimulation. *Brain*. 2021;144(5):1576-1589. doi:awab042

38. Yu T, Wang X, Li Y, et al. High-frequency stimulation of anterior nucleus of thalamus desynchronizes epileptic network in humans. *Brain*. 2018;141(9):2631-2643. doi:10.1093/brain/awy187
39. Dickinson A, Varcin KJ, Sahin M, Nelson CA, Jeste SS. Early patterns of functional brain development associated with autism spectrum disorder in tuberous sclerosis complex. *Autism Res*. 2019;12(12):1758-1773. doi:10.1002/aur.2193
40. Davis PE, Kapur K, Filip-Dhima R, et al. Increased electroencephalography connectivity precedes epileptic spasm onset in infants with tuberous sclerosis complex. *Epilepsia*. 2019;60(8):1721-1732. doi:10.1111/epi.16284
41. Anderson DE, Madhavan D, Swaminathan A. Global brain network dynamics predict therapeutic responsiveness to cannabidiol treatment for refractory epilepsy. *Brain Commun*. 2020;2(2). doi:10.1093/braincomms/fcaa140
42. Zelmann R, Lina JM, Schulze-Bonhage A, Gotman J, Jacobs J. Scalp EEG is not a blur: It can see high frequency oscillations although their generators are small. *Brain Topogr*. 2014;27(5):683-704. doi:10.1007/s10548-013-0321-y
43. Petroff OA, Spencer DD, Goncharova II, Zaveri HP. A comparison of the power spectral density of scalp EEG and subjacent electrocorticograms. *Clin Neurophysiol*. 2016;127(2):1108-1112. doi:10.1016/j.clinph.2015.08.004
44. Hellwig B. A quantitative analysis of the local connectivity between pyramidal neurons in layers 2/3 of the rat visual cortex. *Biol Cybern*. 2000;82(2):111-121. doi:10.1007/PL00007964

Figure Legends

Figure 1. Brain state abnormalities in Syngap$^{+/\Delta\text{-GAP}}$ rats. (A) Schematic of a 32-channel skull-surface EEG implant illustrating approximate location of electrodes relative to the brain (left). Representative EEG voltage and accelerometer traces from numbered electrodes in schematic on left showing examples from NREM, REM and wake states (right). Dotted black lines indicate brain state transitions, grey lines show example 5 sec brain state epochs. Electrode position abbreviations (Supplementary Fig. 1) are displayed to the right of traces. Plots of percent time of 6 hr recording, number of bouts and average bout duration for NREM (B), REM (C) and wake (D) brain states. Bars indicate mean values (mean ± standard error of the mean (SEM)). Points correspond to values from individual rats. Number of bouts was significantly lower, while bout duration was significantly higher in Syngap$^{+/\Delta\text{-GAP}}$ rats (* = p<0.05, ** = p<0.01, *** p = <0.001, **** p = <0.0001, unpaired two-sample t-tests and two-sample Man Whitney-U rank sum tests specified in results text). Power spectrum estimates averaged across all NREM (E), REM (F) and wake (G) epochs. Error bars indicate SEM. Plots of average power in commonly used frequency bands during NREM (H), REM (I) and wake (J). Bars indicate mean values (mean ± SEM). Points correspond to values from individual rats. There were no significant differences across any bands between genotypes (two-way ANOVA specified in results text).

Figure 2. Decreased imaginary coherence during NREM in short-distance (< 2 mm apart) electrode pairs in Syngap$^{+/\Delta\text{-GAP}}$ rats. Average Z' imaginary coherence during NREM (A), REM (D) and wake (G) epochs. Shaded area indicates SEM. Inset in A: schematic of electrode pairs < 2mm apart. Plots of average Z' imaginary coherence in commonly used frequency bands during NREM (B), REM (E) and wake (H). Lines indicate mean values (mean ± SEM). Points correspond to values from individual rats. There were no significant differences across any commonly used bands between genotypes (two-way ANOVA, p = > 0.05). Plots of p-values for cluster-based nonparametric tests during NREM (C), REM (F) and wake (I). Dotted red lines indicate two-sided p-value thresholds of ≥ 0.975 and ≤ 0.025 corresponding to significantly different thresholds equivalent to p ≤ 0.05, two sided. Note: A long cluster of significant frequencies was found during NREM between 11.5 and 29.5 Hz indicating a decrease in Z' imaginary coherence in Syngap$^{+/\Delta\text{-GAP}}$ rats.

Figure 3. Increased imaginary coherence during wake in long-distance (> 2 mm apart) electrode pairs in Syngap$^{+/\Delta\text{-GAP}}$ rats. Average Z' imaginary coherence during REM (A), NREM (D) and wake (G) epochs. Shaded area indicates SEM. Inset in A: schematic of electrode pairs > 2mm apart. Plots of average Z' imaginary coherence in commonly used frequency bands during NREM (B), REM (E) and wake (H). Bars indicate mean values (mean ± SEM). Points correspond to values from individual rats. There were no significant differences across any commonly used bands between genotypes (two-way ANOVA, p = > 0.05). Plots of p-values for cluster-based nonparametric test during NREM (C), REM (F) and wake (I). Dotted red lines indicate two-sided p-value thresholds of ≥ 0.975 and ≤ 0.025 corresponding to significantly different thresholds equivalent to p ≤ 0.05, two sided. Note: Clusters of significant frequencies were found during wake between 8 and 9.5 Hz and 14 and 16.5 Hz indicating an increase in Z' imaginary coherence in Syngap$^{+/\Delta\text{-GAP}}$ rats.

Figure 4. SWDs are uncorrelated to sleep and connectivity abnormalities in Syngap$^{+/\Delta\text{-GAP}}$ animals. (A) Representative EEG traces during a SWD in 5 electrodes in Syngap$^{+/\Delta\text{-GAP}}$ rats. Plots of NREM bouts (B), average NREM bout duration (C), wake bouts (D), average wake bout duration (E), and average Z-1 Imaginary Coherence in the 12-22 Hz band (F) plotted against percentage time of SWD occurrence. Points correspond to values from individual rats and blue is line of best fit. There was a significant correlation between average wake bout duration and percent time in SWDs in Syngap$^{+/\Delta\text{-GAP}}$ rats with no differences in the other metrics (* = p<0.05, Pearson correlation).

Figure 5. Sleep spindles are unaltered in Syngap$^{+/\Delta\text{-GAP}}$ animals. (A) Representative EEG traces during sleep spindles in 16 electrodes in Syngap$^{+/+}$ (left) and Syngap$^{+/\Delta\text{-GAP}}$ (right) rats. Plots of spindle number (B), average duration (C), average amplitude (D), average power in the spindle frequency band (12 – 17 Hz) (E), multi-electrode spindles (F) and average electrodes per spindle (F). Bars indicate mean values (mean ± standard error of the mean (SEM)). Points correspond to values from individual rats. There was a significant decrease in spindle duration in Syngap$^{+/\Delta\text{-GAP}}$ rats with no differences in the other metrics (* = p<0.05, unpaired two-sample t-tests).

Figure 6. The occurrences of high connectivity during sleep spindles was reduced in short-distance (< 2 mm apart) electrode pairs in Syngap$^{+/\Delta\text{-GAP}}$ rats. (A) Average coherograms across electrode pairs preceding and during sleep spindles (top). Magenta dots indicate instances of high connectivity (70% of maximum average connectivity time-frequency bin detected in each animal). Schematic of electrode pairs < 2mm apart and imaginary coherence colour scale (below). Plots of total high connectivity time-frequency bins (B) and average oscillatory frequency of high connectivity pixels per spindle (F). Bars indicate mean values (mean ± SEM). Points correspond to values from individual rats. There was a significant decrease in high connectivity (two-sample unpaired t-test**,** DF = 22, T = -2.39, p=0.03) time-frequency bins and a significant increase in the average oscillatory frequency of high connectivity time-frequency bins (two-sample unpaired t-test, DF = 22, T = 2.13, p=0.04) in Syngap$^{+/\Delta\text{-GAP}}$ animals.

Figure 7**. A specific subset of electrode pairs displays significantly reduced imaginary coherence during sleep spindles in Syngap$^{+/\Delta\text{-GAP}}$ rats.** (A) Schematic of electrodes pairs with a significant reduction in imaginary coherence during sleep spindles in Syngap$^{+/\Delta\text{-GAP}}$ animals. Note: Thickness of lines indicate relative significance level detailed in Supp Table 1. (B) Average imaginary coherence preceding and during sleep spindles for all 496 (top), < 2 mm apart (middle) and individually significant (bottom) electrode pairs (Supp Table 1). Shaded area indicates SEM. (C) Plots of p-values for cluster-based nonparametric test preceding and during sleep spindles for all 496, < 2 mm apart and individually significant electrode pairs. Dotted red lines indicate two-sided p-value thresholds of ≥ 0.975 and ≤ 0.025 corresponding to significantly different thresholds equivalent to p ≤ 0.05. Note: Clusters of significant times

during sleep spindles were primarily found in individually significant electrode pairs in Syngap$^{+/\Delta\text{-GAP}}$ rats. (D) Schematic of regional areas averaged and in which dynamic imaginary coherence was calculated. (E) Plots of average imaginary coherence preceding and during sleep spindles with p-values for cluster-based nonparametric test. Dotted red lines indicate two-sided p-value thresholds of ≥ 0.975 and ≤ 0.025 corresponding to significantly different thresholds equivalent to $p \leq 0.05$, two sided. Note: Clusters of significant times were only found in left middle – right middle, right middle – right caudal and left middle – right caudal comparisons. Other none significant comparisons are displayed in Supplementary Figure 4.

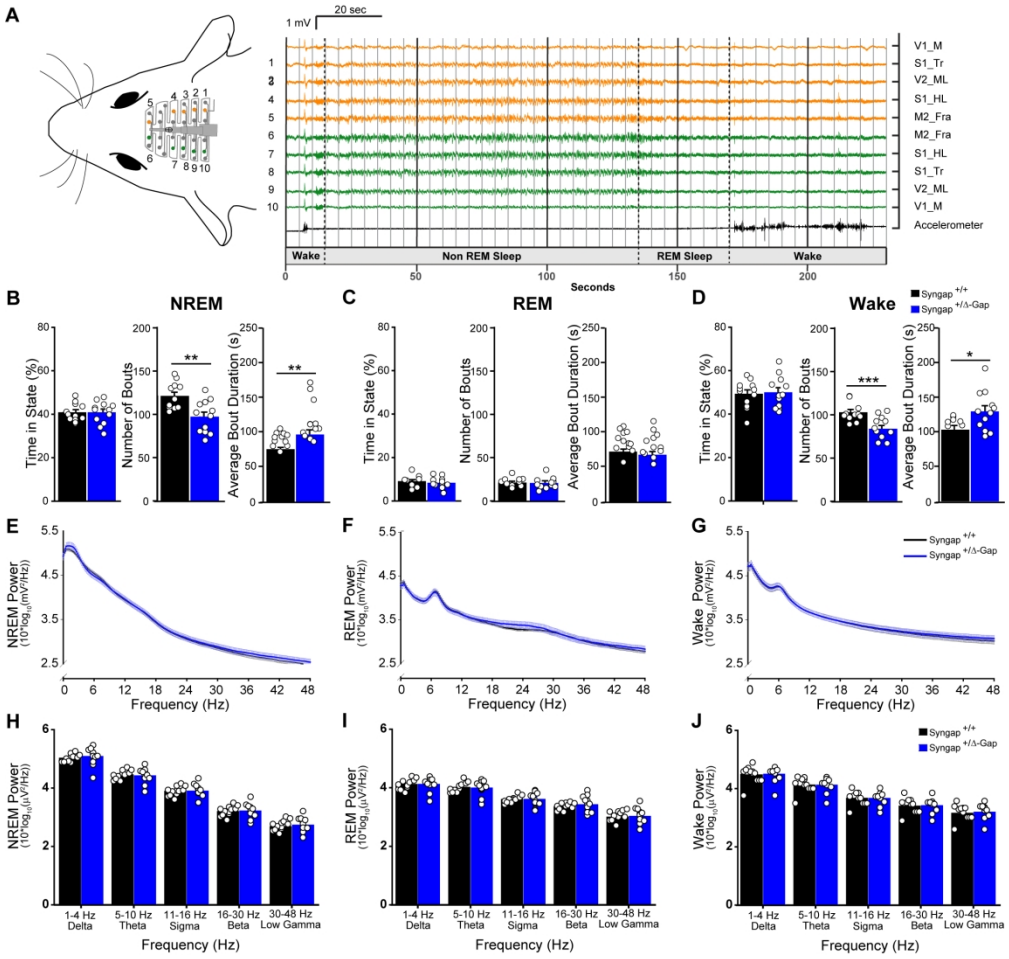

Figure 1. Brain state abnormalities in Syngap+/Δ-GAP rats. (A) Schematic of a 32-channel skull-surface EEG implant illustrating approximate location of electrodes relative to the brain (left). Representative EEG voltage and accelerometer traces from numbered electrodes in schematic on left showing examples from NREM, REM and wake states (right). Dotted black lines indicate brain state transitions, grey lines show example 5 sec brain state epochs. Electrode position abbreviations (Supplementary Fig. 1) are displayed to the right of traces. Plots of percent time of 6 hr recording, number of bouts and average bout duration for NREM (B), REM (C) and wake (D) brain states. Bars indicate mean values (mean ± standard error of the mean (SEM)). Points correspond to values from individual rats. Number of bouts was significantly lower, while bout duration was significantly higher in Syngap+/Δ-GAP rats (* = $p<0.05$, ** = $p<0.01$, *** p = <0.001, **** p = <0.0001, unpaired two-sample t-tests and two-sample Man Whitney-U rank sum tests specified in results text). Power spectrum estimates averaged across all NREM (E), REM (F) and wake (G) epochs. Error bars indicate SEM. Plots of average power in commonly used frequency bands during NREM (H), REM (I) and wake (J). Bars indicate mean values (mean ± SEM). Points correspond to values from individual rats. There were no significant differences across any bands between genotypes (two-way ANOVA specified in results text).

503x478mm (118 x 118 DPI)

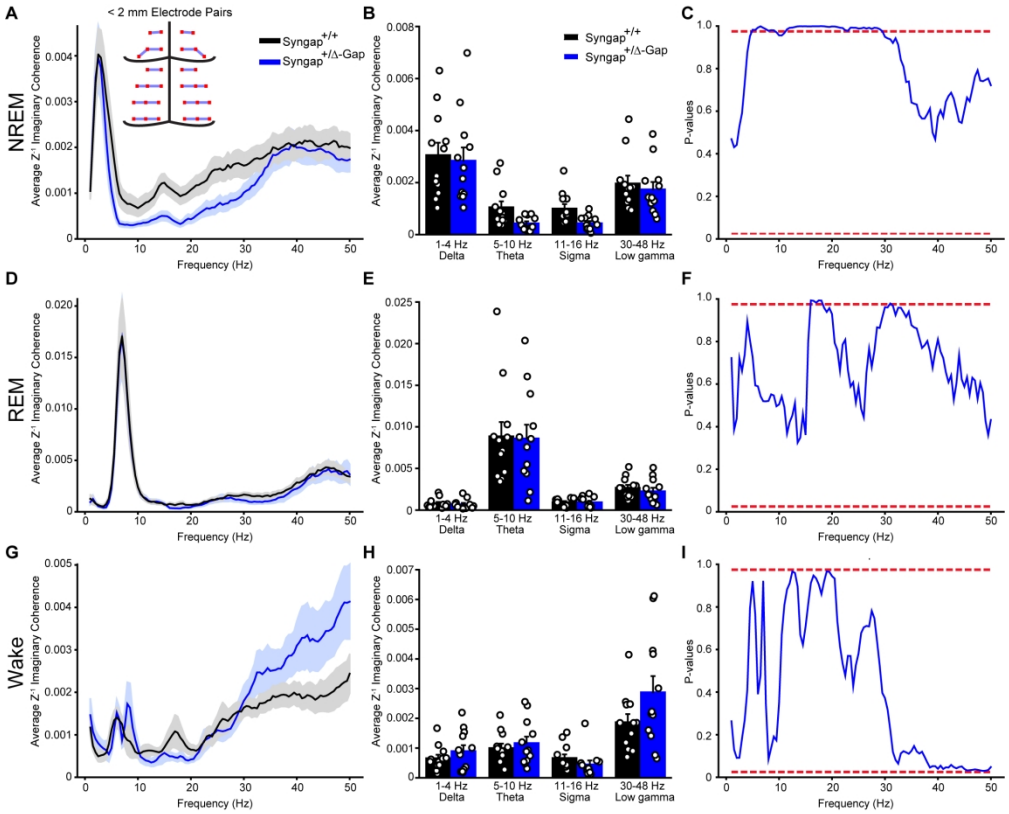

Figure 2. Decreased imaginary coherence during NREM in short-distance (< 2 mm apart) electrode pairs in Syngap+/Δ-GAP rats. Average Z' imaginary coherence during NREM (A), REM (D) and wake (G) epochs. Shaded area indicates SEM. Inset in A: schematic of electrode pairs < 2mm apart. Plots of average Z' imaginary coherence in commonly used frequency bands during NREM (B), REM (E) and wake (H). Lines indicate mean values (mean ± SEM). Points correspond to values from individual rats. There were no significant differences across any commonly used bands between genotypes (two-way ANOVA, p = > 0.05). Plots of p-values for cluster-based nonparametric tests during NREM (C), REM (F) and wake (I). Dotted red lines indicate two-sided p-value thresholds of ≥ 0.975 and ≤ 0.025 corresponding to significantly different thresholds equivalent to p ≤ 0.05, two sided. Note: A long cluster of significant frequencies was found during NREM between 11.5 and 29.5 Hz indicating a decrease in Z' imaginary coherence in Syngap+/Δ-GAP rats.

200x161mm (300 x 300 DPI)

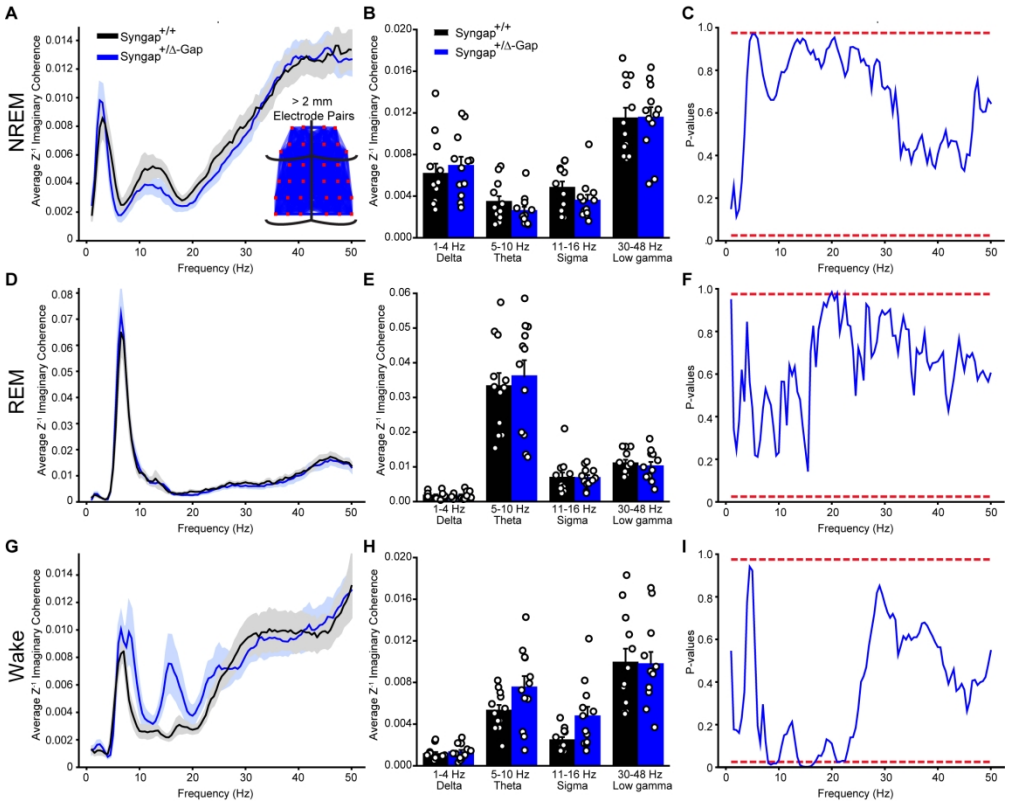

Figure 3. Increased imaginary coherence during wake in long-distance (> 2 mm apart) electrode pairs in Syngap+/Δ-GAP rats. Average Z' imaginary coherence during REM (A), NREM (D) and wake (G) epochs. Shaded area indicates SEM. Inset in A: schematic of electrode pairs > 2mm apart. Plots of average Z' imaginary coherence in commonly used frequency bands during NREM (B), REM (E) and wake (H). Bars indicate mean values (mean ± SEM). Points correspond to values from individual rats. There were no significant differences across any commonly used bands between genotypes (two-way ANOVA, p = > 0.05). Plots of p-values for cluster-based nonparametric test during NREM (C), REM (F) and wake (I). Dotted red lines indicate two-sided p-value thresholds of ≥ 0.975 and ≤ 0.025 corresponding to significantly different thresholds equivalent to p ≤ 0.05, two sided. Note: Clusters of significant frequencies were found during wake between 8 and 9.5 Hz and 14 and 16.5 Hz indicating an increase in Z' imaginary coherence in Syngap+/Δ-GAP rats.

200x159mm (300 x 300 DPI)

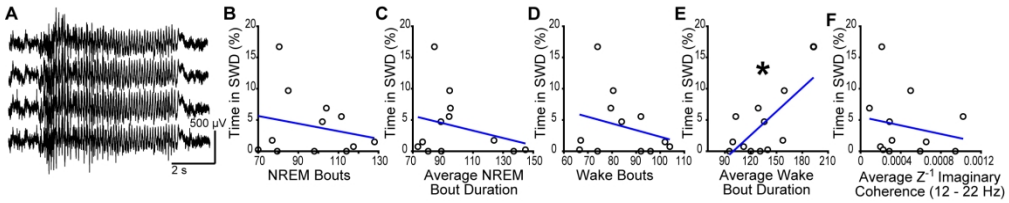

Figure 4. SWDs are uncorrelated to sleep and connectivity abnormalities in Syngap+/Δ-GAP animals. (A) Representative EEG traces during a SWD in 5 electrodes in Syngap+/Δ-GAP rats. Plots of NREM bouts (B), average NREM bout duration (C), wake bouts (D), average wake bout duration (E), and average Z-1 Imaginary Coherence in the 12-22 Hz band (F) plotted against percentage time of SWD occurrence. Points correspond to values from individual rats and blue is line of best fit. There was a significant correlation between average wake bout duration and percent time in SWDs in Syngap+/Δ-GAP rats with no differences in the other metrics (* = $p<0.05$, Pearson correlation).

498x97mm (118 x 118 DPI)

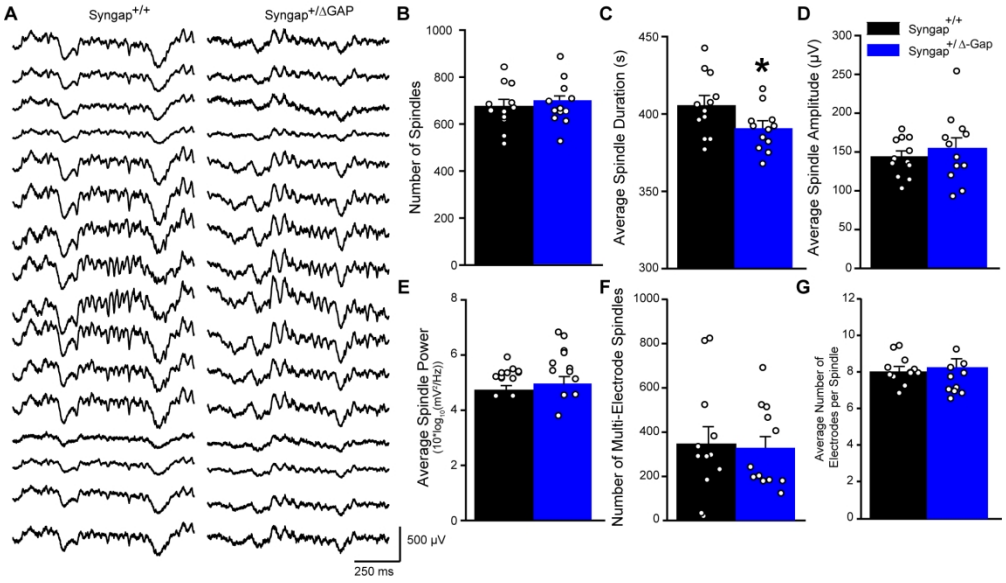

Figure 5. Sleep spindles are unaltered in Syngap+/Δ-GAP animals. (A) Representative EEG traces during sleep spindles in 16 electrodes in Syngap+/+ (left) and Syngap+/Δ-GAP (right) rats. Plots of spindle number (B), average duration (C), average amplitude (D), average power in the spindle frequency band (12 – 17 Hz) (E), multi-electrode spindles (F) and average electrodes per spindle (F). Bars indicate mean values (mean ± standard error of the mean (SEM)). Points correspond to values from individual rats. There was a significant decrease in spindle duration in Syngap+/Δ-GAP rats with no differences in the other metrics (* = $p<0.05$, unpaired two-sample t-tests).

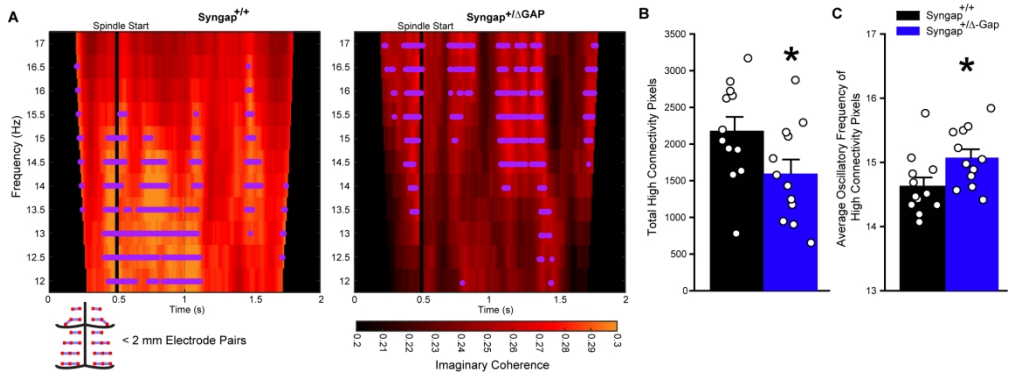

Figure 6. The occurrences of high connectivity during sleep spindles was reduced in short-distance (< 2 mm apart) electrode pairs in Syngap+/Δ-GAP rats. (A) Average coherograms across electrode pairs preceding and during sleep spindles (top). Magenta dots indicate instances of high connectivity (70% of maximum average connectivity time-frequency bin detected in each animal). Schematic of electrode pairs < 2mm apart and imaginary coherence colour scale (below). Plots of total high connectivity time-frequency bins (B) and average oscillatory frequency of high connectivity pixels per spindle (F). Bars indicate mean values (mean ± SEM). Points correspond to values from individual rats. There was a significant decrease in high connectivity (two-sample unpaired t-test, DF = 22, T = -2.39, p=0.03) time-frequency bins and a significant increase in the average oscillatory frequency of high connectivity time-frequency bins (two-sample unpaired t-test, DF = 22, T = 2.13, p=0.04) in Syngap+/Δ-GAP animals.

200x74mm (300 x 300 DPI)

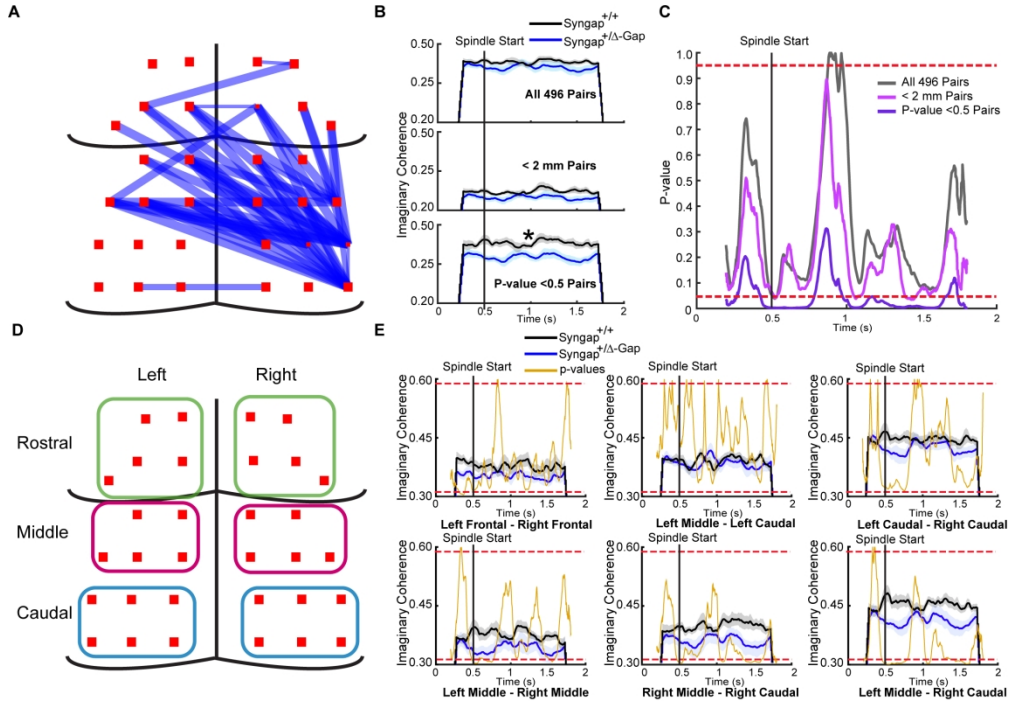

Figure 7. A specific subset of electrode pairs displays significantly reduced imaginary coherence during sleep spindles in Syngap+/Δ-GAP rats. (A) Schematic of electrodes pairs with a significant reduction in imaginary coherence during sleep spindles in Syngap+/Δ-GAP animals. Note: Thickness of lines indicate relative significance level detailed in Supp Table 1. (B) Average imaginary coherence preceding and during sleep spindles for all 496 (top), < 2 mm apart (middle) and individually significant (bottom) electrode pairs (Supp Table 1). Shaded area indicates SEM. (C) Plots of p-values for cluster-based nonparametric test preceding and during sleep spindles for all 496, < 2 mm apart and individually significant electrode pairs. Dotted red lines indicate two-sided p-value thresholds of ≥ 0.975 and ≤ 0.025 corresponding to significantly different thresholds equivalent to $p \leq 0.05$. Note: Clusters of significant times during sleep spindles were primarily found in individually significant electrode pairs in Syngap+/Δ-GAP rats. (D) Schematic of regional areas averaged and in which dynamic imaginary coherence was calculated. (E) Plots of average imaginary coherence preceding and during sleep spindles with p-values for cluster-based nonparametric test. Dotted red lines indicate two-sided p-value thresholds of ≥ 0.975 and ≤ 0.025 corresponding to significantly different thresholds equivalent to $p \leq 0.05$, two sided. Note: Clusters of significant times were only found in left middle – right middle, right middle – right caudal and left middle – right caudal comparisons. Other non-significant comparisons are displayed in Supplementary Figure 4.

510x358mm (118 x 118 DPI)

Supplementary Material

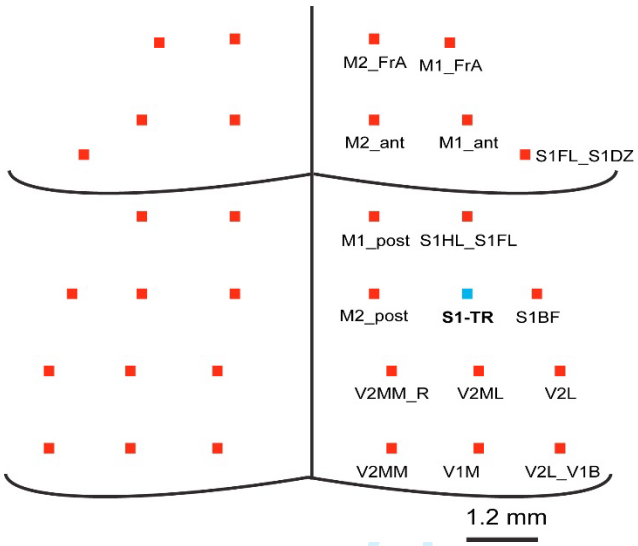

Supp Fig 1. Diagram of approximate electrode location and abbreviations of approximate underlying cortical areas.
Coordinates were based on approximate locations from (Paxinos and Watson, 1998)

V2L_V1B: Secondary visual cortex lateral area – Primary visual cortex binocular area
V1M: Primary visual cortex monocular area
V2MM: Secondary visual cortex mediomedial area
V2L: Secondary visual lateral area
V2ML: Secondary visual mediolateral area
V2MM_R: Secondary visual cortex mediomedial area - retrosplenial agranular area
S1DZ_S1BF: Primary somatosensory cortex barrel Field
S1Tr: Primary somatosensory cortex trunk area
M2_post: Posterior secondary motor cortex
S1HL_S1FL: Primary somatosensory cortex hindlimb region – forelimb region
M1_post: Posterior primary motor cortex
S1FL_S1DZ: Primary somatosensory cortex forelimb region - disgranular region
M1_ant: Anterior primary motor cortex
M2_ant: Anterior secondary motor cortex
M1_FrA: Primary motor cortex – frontal association cortex
M2_FrA: Secondary motor cortex – frontal association cortex

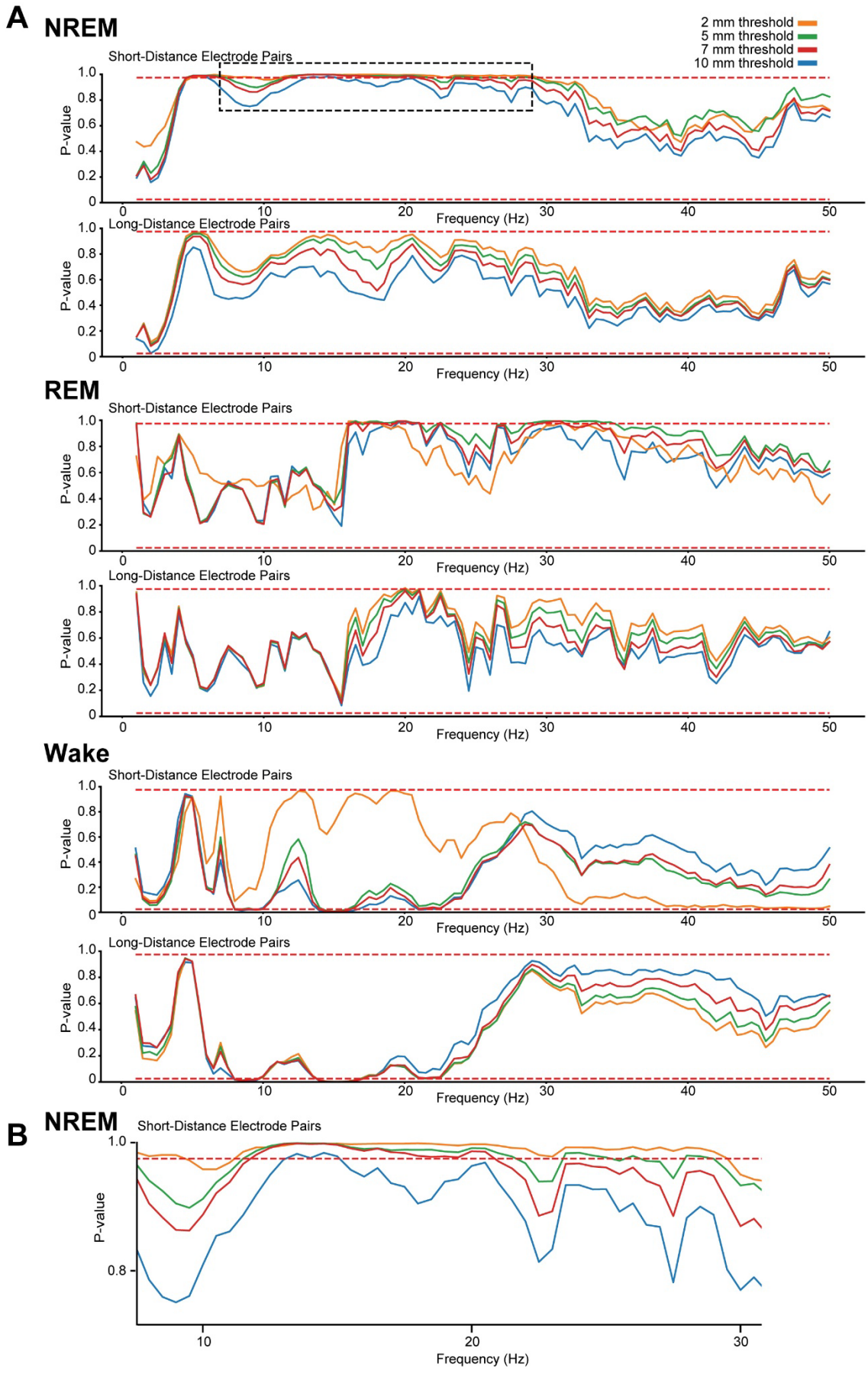
A
NREM
2 mm threshold
5 mm threshold
7 mm threshold
10 mm threshold
Short-Distance Electrode Pairs
Long-Distance Electrode Pairs
P-value
Frequency (Hz)
REM
Short-Distance Electrode Pairs
Long-Distance Electrode Pairs
Wake
Short-Distance Electrode Pairs
Long-Distance Electrode Pairs
B
NREM
Short-Distance Electrode Pairs

Supp Fig. 2. Plots of p-values at multiple distance thresholds. (A) P-values of differences at individual frequencies comparing imaginary coherence between *Syngap*$^{+/\Delta\text{-}GAP}$ and *Syngap*$^{+/+}$ rats for cluster-based nonparametric tests for short and long distance electrodes during NREM, REM and wake. Dotted red lines indicate two-sided p-vale thresholds of ≥ 0.975 and ≤ 0.025 corresponding to significantly different thresholds equivalent to $p \leq 0.05$. Note: The distance threshold determines how electrode combinations are grouped as short or long distance combinations. At thresholds of 2, 5, 7 and 10 mm there were 20, 170, 284 and 432 electrodes in the short distance groups and 476, 326, 212 and 64 electrodes in the long distance groups respectively. (B) Expanded p-value and frequency plot of area within the dotted black rectangle in (A). Note: A long cluster of significant frequencies was found during NREM between 11.5 and 29.5 Hz in electrodes ≤ 2mm indicating a decrease in Z' imaginary coherence in *Syngap*$^{+/\Delta\text{-}GAP}$ rats. The longest consecutively significant frequencies clusters are present amongst short-distance electrodes ≤ 2mm apart.

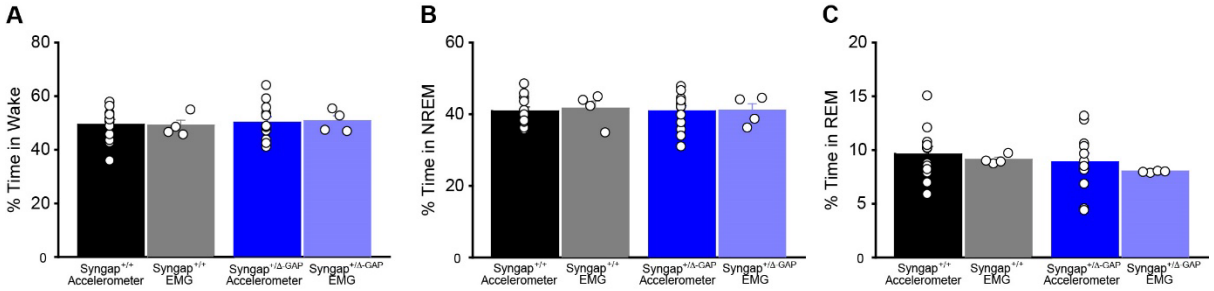

Supp Fig. 3. Validation of visual scoring obtained through EEG with head accelerometer against standard EEG+EMG. (A) Comparison of percentage of time in Wake, (B) NREM and (C) REM, obtained by visual scoring with accelerometer (Fig. 1B) with 4 *Syngap*$^{+/\Delta\text{-}GAP}$ and 4 *Syngap*$^{+/+}$ rats recorded with EEG+EMG (see methods). Two-way ANOVA for independent measures did not reveal significant differences for factor Genotype, factor Method, or for the interaction between Genotype x Method. Comparison between genotypes for the results obtained using the EMG+EEG method did not show significant differences for percentage in Wake (2-tailed t-test: DF = 6, T= 0.581, p=0.583; *Syngap*$^{+/+}$: 49.15 ± 1.82; *Syngap*$^{+/\Delta\text{-}GAP}$: 49.15 ± 1.82), NREM (unpaired 2-tailed t-test: DF = 6, T= 0.193, p=0.853; *Syngap*$^{+/+}$: 41.7 ± 1.98; *Syngap*$^{+/\Delta\text{-}GAP}$: 41.11 ± 1.78), or REM (unpaired 2-tailed t-test: DF = 6, T= 0.174, p=0.868; *Syngap*$^{+/+}$: 9.14 ± 0.19; *Syngap*$^{+/\Delta\text{-}GAP}$: 8.03 ± 0.03), thus confirming the trend found using accelerometer. Bars indicate mean values (mean ± SEM). Points correspond to values from individual rats.

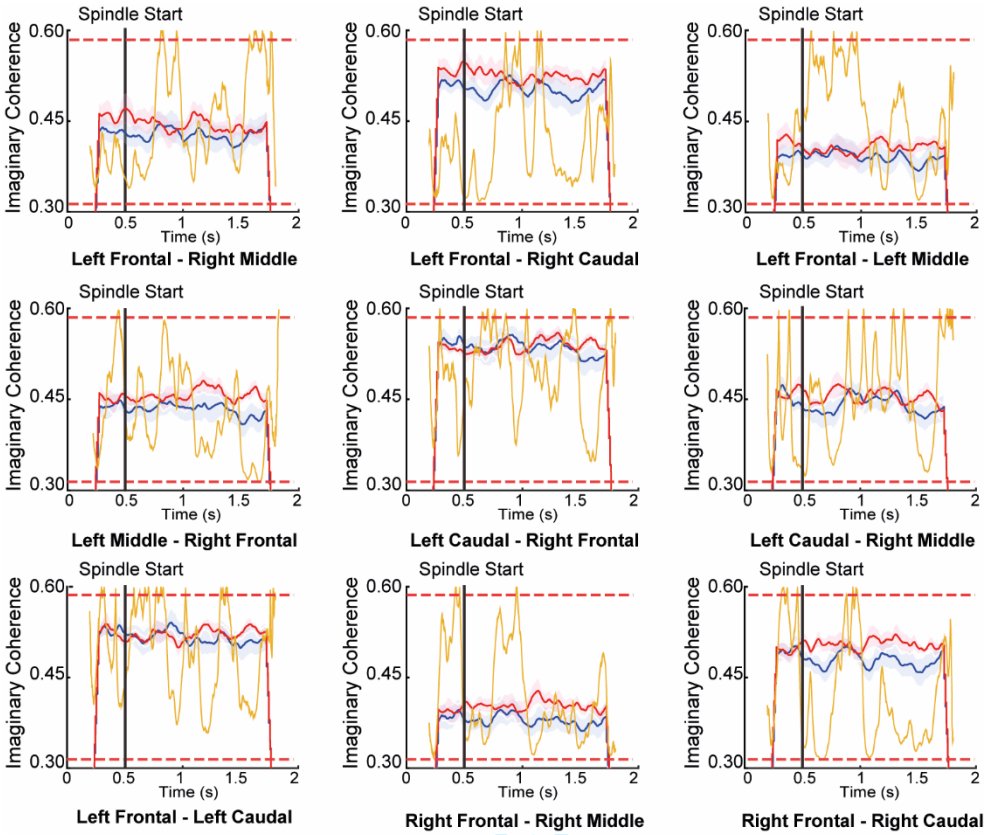

Supp Fig. 4. Plots comparing average imaginary coherence preceding and during sleep spindles between *Syngap*$^{+/\Delta\text{-}GAP}$ and *Syngap*$^{+/+}$ rats. P-values for cluster-based nonparametric test displayed in yellow with dotted red lines indicating two-sided p-value thresholds of ≥ 0.975 and ≤ 0.025 corresponding to significantly different thresholds equivalent to p ≤ 0.05, two sided. Note: Comparison schematic and other comparisons are displayed in main text Fig. 7.

Supp Table 1. Electrode pairs during sleep spindles with significantly decreased dynamic imaginary coherence. All 496 electrode pairs were compared across animals with a two-sample t-test. The 45 significant pairs are listed below with corresponding p-values.

Electrode Pairs		p-values
V2L_V1B_RIGHT	S1Tr_LEFT	0.031
V2L_RIGHT	S1Tr_LEFT	0.033
V2ML_RIGHT	S1Tr_LEFT	0.031
V2MM_RSA_RIGHT	S1Tr_LEFT	0.049
M2_ant_RIGHT	S1DZ_S1BF_LEFT	0.042
V2L_V1B_RIGHT	S1DZ_S1BF_LEFT	0.003
V2L_RIGHT	S1DZ_S1BF_LEFT	0.007
V2ML_RIGHT	S1DZ_S1BF_LEFT	0.050
S1DZ_S1BF_RIGHT	S1DZ_S1BF_LEFT	0.035
V2MM_RIGHT	V1M_LEFT	0.035
V2L_V1B_RIGHT	M2_post_LEFT	0.028
V2L_RIGHT	M2_post_LEFT	0.038
V2MM_RSA_RIGHT	M2_post_LEFT	0.028
V2L_V1B_RIGHT	S1HL_S1FL_LEFT	0.050
V2L_RIGHT	S1HL_S1FL_LEFT	0.043
V2L_V1B_RIGHT	M1_post_LEFT	0.017
V2L_RIGHT	M1_post_LEFT	0.017
V2ML_RIGHT	M1_post_LEFT	0.031
V2MM_RSA_RIGHT	M1_post_LEFT	0.040
S1DZ_S1BF_RIGHT	M1_post_LEFT	0.029
V2L_RIGHT	S1FL_S1DZ_LEFT	0.049
M1_FrA_RIGHT	M1_ant_LEFT	0.033
V2L_V1B_RIGHT	M1_ant_LEFT	0.036
V2L_RIGHT	M1_ant_LEFT	0.041
M2_ant_RIGHT	M2_ant_LEFT	0.029
V2L_V1B_RIGHT	M2_ant_LEFT	0.021
V2L_RIGHT	M2_ant_LEFT	0.022
S1DZ_S1BF_RIGHT	M2_ant_LEFT	0.037
M1_FrA_RIGHT	M2_FrA_RIGHT	0.046
V2L_V1B_RIGHT	M2_ant_RIGHT	0.018
V2L_RIGHT	M2_ant_RIGHT	0.020
S1DZ_S1BF_RIGHT	M2_ant_RIGHT	0.020
V2L_RIGHT	M1_ant_RIGHT	0.026
S1DZ_S1BF_RIGHT	M1_ant_RIGHT	0.042
V2L_RIGHT	S1FL_S1DZ_RIGHT	0.025
S1DZ_S1BF_RIGHT	S1FL_S1DZ_RIGHT	0.044
V2L_V1B_RIGHT	M1_post_RIGHT	0.015
V2L_RIGHT	M1_post_RIGHT	0.008
V2ML_RIGHT	M1_post_RIGHT	0.037
S1DZ_S1BF_RIGHT	M1_post_RIGHT	0.004
V2L_RIGHT	V2L_V1B_RIGHT	0.002
V2ML_RIGHT	V2L_V1B_RIGHT	0.038
S1DZ_S1BF_RIGHT	V2L_V1B_RIGHT	0.008
S1Tr_RIGHT	V2L_V1B_RIGHT	0.023
S1Tr_RIGHT	V2L_RIGHT	0.020

The ARRIVE Guidelines Checklist

Animal Research: Reporting In Vivo Experiments

Carol Kilkenny[1], William J Browne[2], Innes C Cuthill[3], Michael Emerson[4] and Douglas G Altman[5]

[1]The National Centre for the Replacement, Refinement and Reduction of Animals in Research, London, UK, [2]School of Veterinary Science, University of Bristol, Bristol, UK, [3]School of Biological Sciences, University of Bristol, Bristol, UK, [4]National Heart and Lung Institute, Imperial College London, UK, [5]Centre for Statistics in Medicine, University of Oxford, Oxford, UK.

	ITEM	RECOMMENDATION	Section/ Paragraph
Title	1	Provide as accurate and concise a description of the content of the article as possible.	Title
Abstract	2	Provide an accurate summary of the background, research objectives, including details of the species or strain of animal used, key methods, principal findings and conclusions of the study.	Abstract
INTRODUCTION			
Background	3	a. Include sufficient scientific background (including relevant references to previous work) to understand the motivation and context for the study, and explain the experimental approach and rationale. b. Explain how and why the animal species and model being used can address the scientific objectives and, where appropriate, the study's relevance to human biology.	Introduction
Objectives	4	Clearly describe the primary and any secondary objectives of the study, or specific hypotheses being tested.	Introduction, Results
METHODS			
Ethical statement	5	Indicate the nature of the ethical review permissions, relevant licences (e.g. Animal [Scientific Procedures] Act 1986), and national or institutional guidelines for the care and use of animals, that cover the research.	Methods - Animals
Study design	6	For each experiment, give brief details of the study design including: a. The number of experimental and control groups. b. Any steps taken to minimise the effects of subjective bias when allocating animals to treatment (e.g. randomisation procedure) and when assessing results (e.g. if done, describe who was blinded and when). c. The experimental unit (e.g. a single animal, group or cage of animals). A time-line diagram or flow chart can be useful to illustrate how complex study designs were carried out.	Methods – Animals, Surgeyr, EEG Recordings.
Experimental procedures	7	For each experiment and each experimental group, including controls, provide precise details of all procedures carried out. For example: a. How (e.g. drug formulation and dose, site and route of administration, anaesthesia and analgesia used [including monitoring], surgical procedure, method of euthanasia). Provide details of any specialist equipment used, including supplier(s). b. When (e.g. time of day). c. Where (e.g. home cage, laboratory, water maze). d. Why (e.g. rationale for choice of specific anaesthetic, route of administration, drug dose used).	Methods – Animals, Surgery, EEG Recordings
Experimental animals	8	a. Provide details of the animals used, including species, strain, sex, developmental stage (e.g. mean or median age plus age range) and weight (e.g. mean or median weight plus weight range). b. Provide further relevant information such as the source of animals, international strain nomenclature, genetic modification status (e.g. knock-out or transgenic), genotype, health/immune status, drug or test naïve, previous procedures, etc.	Methods - Animals

The ARRIVE guidelines. Originally published in *PLoS Biology*, June 2010[1]

Housing and husbandry	9	Provide details of: a. Housing (type of facility e.g. specific pathogen free [SPF]; type of cage or housing; bedding material; number of cage companions; tank shape and material etc. for fish). b. Husbandry conditions (e.g. breeding programme, light/dark cycle, temperature, quality of water etc for fish, type of food, access to food and water, environmental enrichment). c. Welfare-related assessments and interventions that were carried out prior to, during, or after the experiment.	Methods – Animals, Surgery, EEG Recordings
Sample size	10	a. Specify the total number of animals used in each experiment, and the number of animals in each experimental group. b. Explain how the number of animals was arrived at. Provide details of any sample size calculation used. c. Indicate the number of independent replications of each experiment, if relevant.	Methods – Animals, Statistics
Allocating animals to experimental groups	11	a. Give full details of how animals were allocated to experimental groups, including randomisation or matching if done. b. Describe the order in which the animals in the different experimental groups were treated and assessed.	Methods - Animals
Experimental outcomes	12	Clearly define the primary and secondary experimental outcomes assessed (e.g. cell death, molecular markers, behavioural changes).	Results - sleep, connectivity, spindles, dynamic connectivity sections.
Statistical methods	13	a. Provide details of the statistical methods used for each analysis. b. Specify the unit of analysis for each dataset (e.g. single animal, group of animals, single neuron). c. Describe any methods used to assess whether the data met the assumptions of the statistical approach.	Methods – Statistics, Results - Results - sleep, connectivity, spindles, dynamic connectivity sections.
RESULTS			
Baseline data	14	For each experimental group, report relevant characteristics and health status of animals (e.g. weight, microbiological status, and drug or test naïve) prior to treatment or testing. (This information can often be tabulated).	Methods - Animals
Numbers analysed	15	a. Report the number of animals in each group included in each analysis. Report absolute numbers (e.g. 10/20, not 50%[2]). b. If any animals or data were not included in the analysis, explain why.	Results - sleep, connectivity, spindles, dynamic connectivity sections. No animals were excluded.
Outcomes and estimation	16	Report the results for each analysis carried out, with a measure of precision (e.g. standard error or confidence interval).	Results - sleep, connectivity, spindles, dynamic connectivity sections.
Adverse events	17	a. Give details of all important adverse events in each experimental group. b. Describe any modifications to the experimental protocols made to reduce adverse events.	No adverse effects were detected.

DISCUSSION			
Interpretation/ scientific implications	18	a. Interpret the results, taking into account the study objectives and hypotheses, current theory and other relevant studies in the literature. b. Comment on the study limitations including any potential sources of bias, any limitations of the animal model, and the imprecision associated with the results[2]. c. Describe any implications of your experimental methods or findings for the replacement, refinement or reduction (the 3Rs) of the use of animals in research.	Results - sleep, connectivity, spindles, dynamic connectivity sections. Discussion
Generalisability/ translation	19	Comment on whether, and how, the findings of this study are likely to translate to other species or systems, including any relevance to human biology.	Introduction, Discussion.
Funding	20	List all funding sources (including grant number) and the role of the funder(s) in the study.	Methods - Funding

References:
1. Kilkenny C, Browne WJ, Cuthill IC, Emerson M, Altman DG (2010) Improving Bioscience Research Reporting: The ARRIVE Guidelines for Reporting Animal Research. *PLoS Biol* 8(6): e1000412. doi:10.1371/journal.pbio.1000412
2. Schulz KF, Altman DG, Moher D, the CONSORT Group (2010) CONSORT 2010 Statement: updated guidelines for reporting parallel group randomised trials. *BMJ* 340:c332.